Supporting Information

General Synthetic Strategy for Libraries of Supported Multicomponent Metal Nanoparticles

Hui Yang,[†,§,#] Siobhan J. Bradley,[‡] Xin Wu,[§] Andrew Chan,[∥] Geoffrey I. N. Waterhouse,[∥] Thomas Nann,[‡]

Jian Zhang,*[,§] Paul E. Kruger,*[,⊥] Shengqian Ma,*[,#] and Shane G. Telfer*[,†]

[†]MacDiarmid Institute for Advanced Materials and Nanotechnology, Institute of Fundamental Sciences, Massey University, Palmerston North 4442, New Zealand.
E-mail: s.telfer@massey.ac.nz

[‡]MacDiarmid Institute for Advanced Materials and Nanotechnology, School of Chemical and Physical Sciences, Victoria University of Wellington, Wellington 6140, New Zealand.

[§]State Key Laboratory of Structural Chemistry, Fujian Institute of Research on the Structure of Matter, Chinese Academy of Sciences, 350002 Fuzhou, P. R. China
E−mail: zhj@fjirsm.ac.cn

[∥]MacDiarmid Institute for Advanced Materials and Nanotechnology, School of Chemical Sciences, The University of Auckland, Auckland 1142, New Zealand.

[⊥]MacDiarmid Institute for Advanced Materials and Nanotechnology, School of Physical and Chemical Sciences, University of Canterbury, Christchurch 8140, New Zealand.
E−mail: paul.kruger@canterbury.ac.nz

[#]Department of Chemistry, University of South Florida, CHE205A, 4202E. Fowler Avenue, Tampa, Florida, 33620, U.S.A.
E−mail: sqma@usf.edu

1. Chemicals

All starting compounds and solvents were used as obtained from commercial sources without further purification unless otherwise noted.

2. Instrumentation

Powder X-ray diffraction (PXRD) were performed on Rigaku X-ray diffractometer with Cu Kα source and Bruker AXS X-ray diffractometer with Cu Kα source. BET surface areas were determined from N_2 adsorption/desorption isotherms at 77 K using automatic volumetric adsorption equipment (Quantachrome, Autosorb iQ_2) and Micromeritics ASAP2020 after pre-treatment under vacuum at 100 °C for 5 h. Scanning Electron Microscope (SEM) images and energy dispersive spectra (EDS) were recorded on a FEI Quanta 200 Environmental Scanning Electron Microscope and Hitachi 800 Scanning Electron Microscope with an EDS module. Transmission Electron Microscope (TEM) images were recorded on FEI Tecnai G^2 BioTwin Transmission Electron Microscope with operating voltage at an accelerating voltage of 100 kV. Scanning Transmission Electron Microscopy (STEM), High Resolution Transmission Electron Microscopic (HRTEM) analysis were carried out with JEOL JEM-2100F Transmission Electron Microscope with operating voltage at an accelerating voltage of 200 kV. EDS line scan analyses were performed on a Tecnai F20 Transmission Electron Microscope with operating voltage at an accelerating voltage of 200 kV. Inductively coupled plasma atomic emission spectroscopy (ICP−AES) on an obin Yvon Horiba−Ultima 2 spectrometer system. Elemental Analyses (EA) were performed on a Vario MICRO analysis system. Raman spectra were measured from powder samples with a Cobalt Samba single-mode 532 nm diode laser on quartz substrates. X-ray Photoelectron Spectroscopy (XPS) analyses were performed using Kratos Axis DLD spectrometer. Fourier transform infrared spectra (FTIR) were recorded on a ThermoElectron Nicolet high-resolution FT-MIR/FT-FarIR. The HER and OER tests were performed with a pine electrochemical analyser (AFMSRCE Electrode Rotator WaveDriver 20 Bipotentiostat/Galvanostat System, USA).

3. Synthetic procedures

Synthesis of polyhedral ZIF-8 nanocrystals

ZIF-8 polyhedra were prepared using a reported procedure with a slight modification.[1] In a typical synthesis, 2-methylimidazole (4.0 g) was dissolved in methanol (MeOH, 60 mL) to form a clear solution. $Zn(NO_3)_2{\cdot}6H_2O$ (1.68 g) in MeOH (20 mL) was added into above solution followed by vigorous stirring for 1 h. The mixture was then incubated at room temperature without stirring. After 24 h, the product was isolated as a white powder by centrifugation and washed several times with deionized water and MeOH, and finally dried overnight under vacuum. Yield = 1.06 g. Analytical and spectroscopic data (*vide infra*) were consistent with those previously reported for ZIF-8.

Synthesis of 2.8 nm PVP-stabilized Pt nanoparticles

2.8 nm PVP-stabilized Pt nanoparticles (PtNPs) were synthesized using a reported procedure with a slight modification.[2] A mixture of PVP (533 mg, Mw = 40,000), MeOH (180 mL), and an aqueous solution of H_2PtCl_6 (6.0 mM, 20 mL) were placed in a flask (500 mL) and refluxed for 3 h under air. The methanol was then removed under reduced pressure. The resulting aqueous dispersion of Pt nanoparticles was stored for further use.

Synthesis of the ZIF/Pt composites

ZIF-8 polyhedra (0.2 g) were dispersed in of MeOH (80 mL) by sonication for 30 min and stirred at room temperature for 1 h. Subsequently, aliquot of the above solution of PtNPs (1.2 mL) was added with vigorous stirring for 4 h. The mixture was then incubated at room temperature without stirring. After 24 h, the product was isolated as a light grey powder by centrifugation and washed several times with deionized water and MeOH, and finally dried overnight under vacuum.

Table S1. Summary of the composition of the precursor materials.

material	Zn wt%	Pt[a] wt%	Ni wt%	M_1[b] wt%	M_2 wt%
ZIF-8@Ni-TA	27.01	n/a	4.32	n/a	n/a
ZIF-8/Pt@K-TA	27.43	1.66	n/a	2.43	n/a
ZIF-8/Pt@Ni-TA	27.80	1.59	3.98	n/a	n/a
ZIF-8/Pt@NiFe-TA	27.28	1.44	2.23	0.95	n/a
ZIF-8/Pt@NiCo-TA	27.20	1.50	2.94	0.52	n/a
ZIF-8/Pt@NiTb-TA	27.51	1.53	2.72	2.24	n/a
ZIF-8/Pt@NiCu-TA	27.41	1.55	2.83	0.76	n/a
ZIF-8/Pt@NiMn-TA	27.83	1.54	3.06	0.18	n/a
ZIF-8/Pt@NiCuFe-TA	28.15	1.56	2.56	0.59	0.42
ZIF-8/Pt@NiCuTb-TA	28.25	1.60	2.49	0.51	0.96

[a] n/a = not applicable; n/d = not determined. [b] M_1 = K, Fe, Co Tb, Cu or Mn; [b] M_2 = Fe or Tb; metal content determined by ICP-AES.

4. Materials characterization

4.1 Photographs

Figure S1. Photographs of (a) ZIF-8/Pt; (b) ZIF-8/Pt@K-TA; (c) ZIF-8/Pt@Ni-TA; (d) ZIF-8/Pt@NiCo-TA; (e) ZIF-8/Pt@NiCu-TA; (f) ZIF-8/Pt@NiFe-TA; (g) ZIF-8/Pt@NiTb-TA; (h) ZIF-8/Pt@NiMn-TA; (i) ZIF-8/Pt@NiCuTb-TA; (j) ZIF-8/Pt@NiCuFe-TA.

4.2 Powder X-ray Diffraction (PXRD)

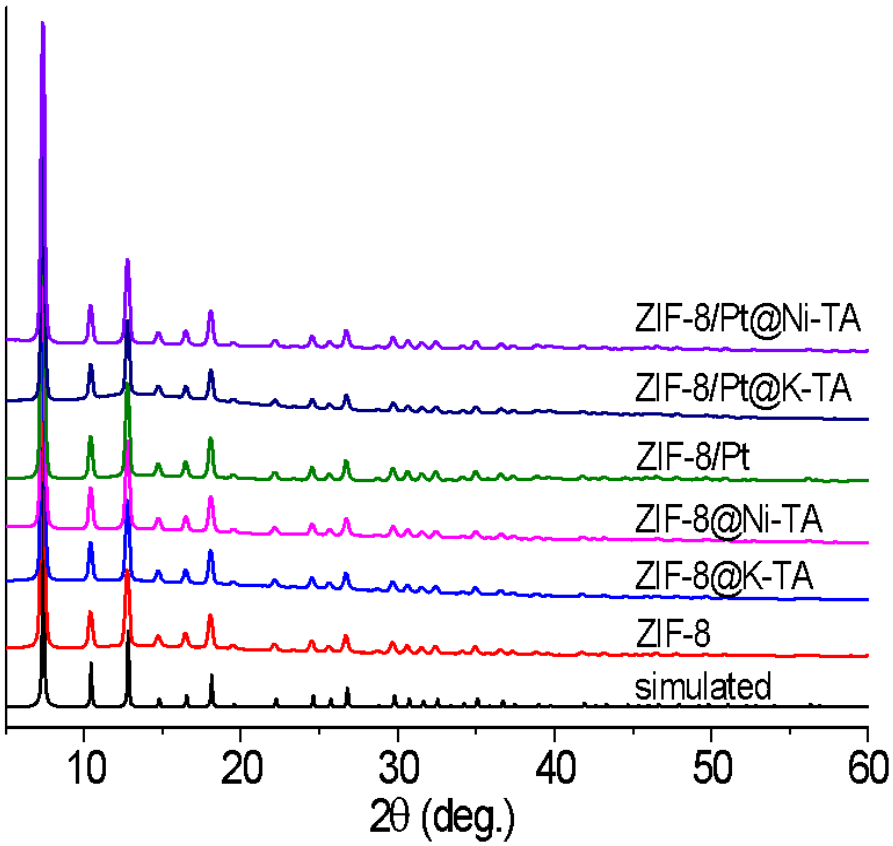

Figure S2. PXRD patterns of the as-synthesized materials.

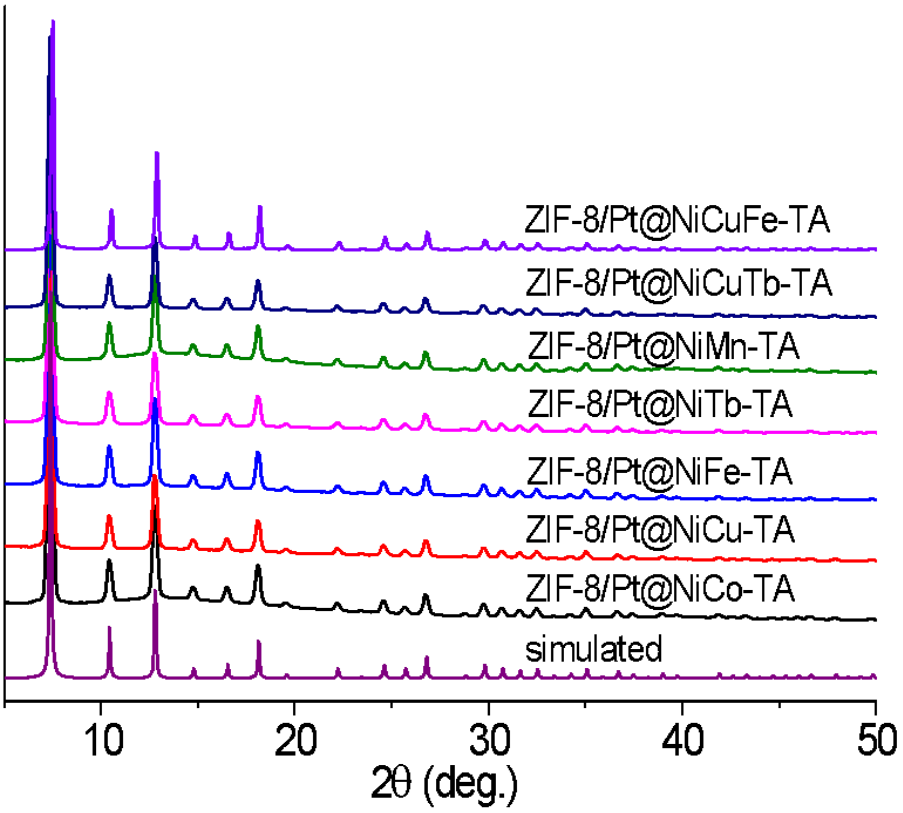

Figure S3. PXRD patterns of the as-synthesized materials.

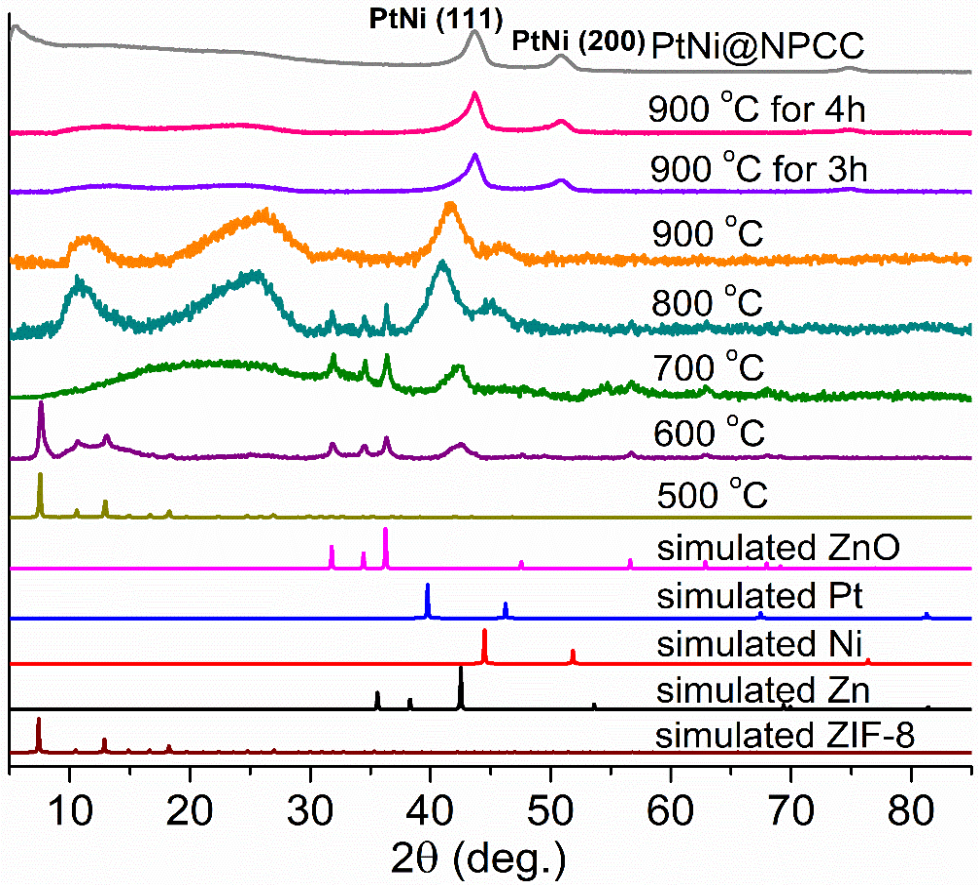

Figure S4. PXRD patterns of ZIF-8/Pt@Ni-TA calcined at different temperatures.

4.3 Scanning Electron Microscopy (SEM) and Transmission Electron Microscopy (TEM)

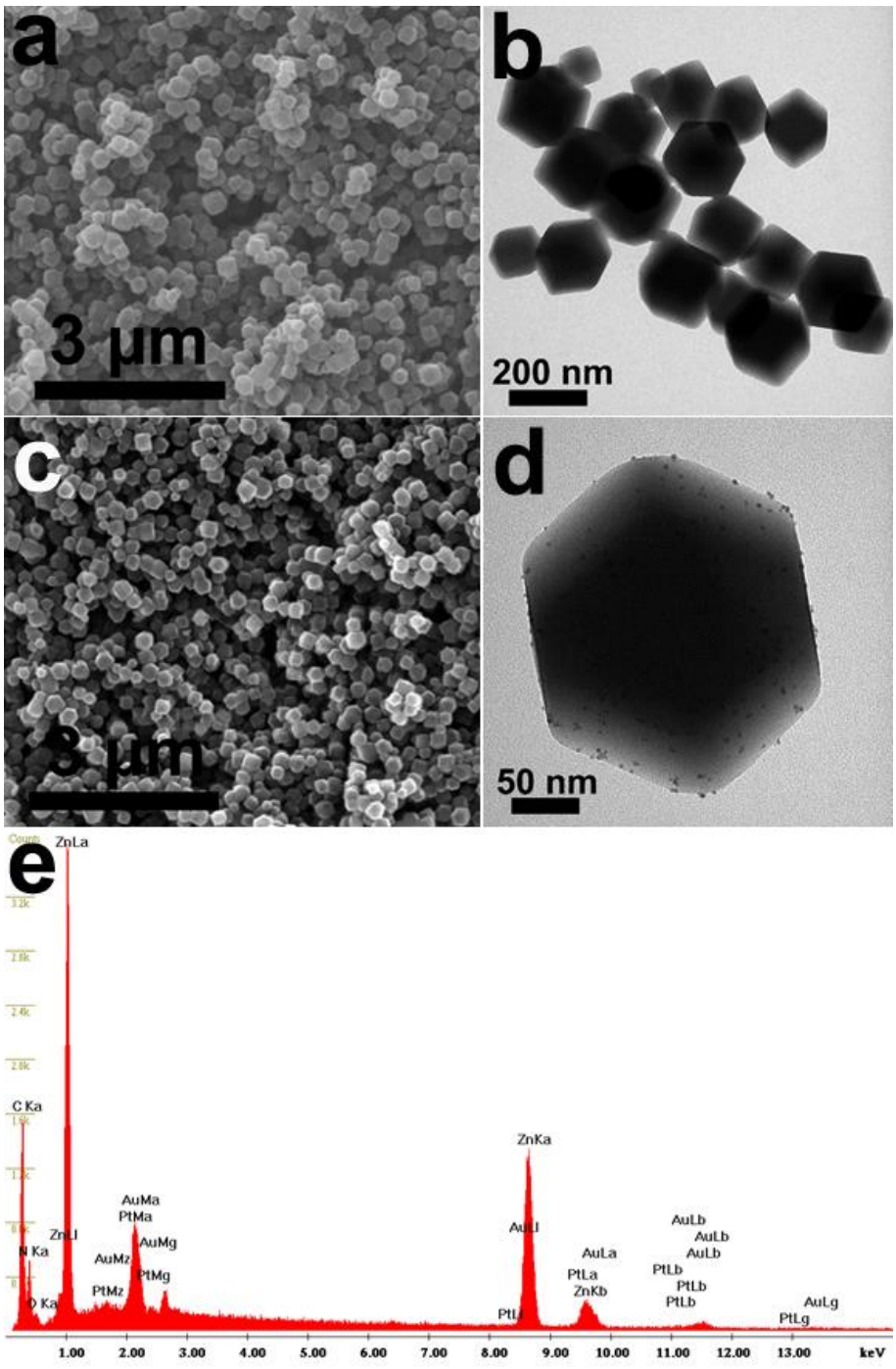

Figure S5. SEM, TEM images and EDS spectrum of polyhedral ZIF-8 (a, b) and ZIF-8/Pt nanocrystals (c, d, e).

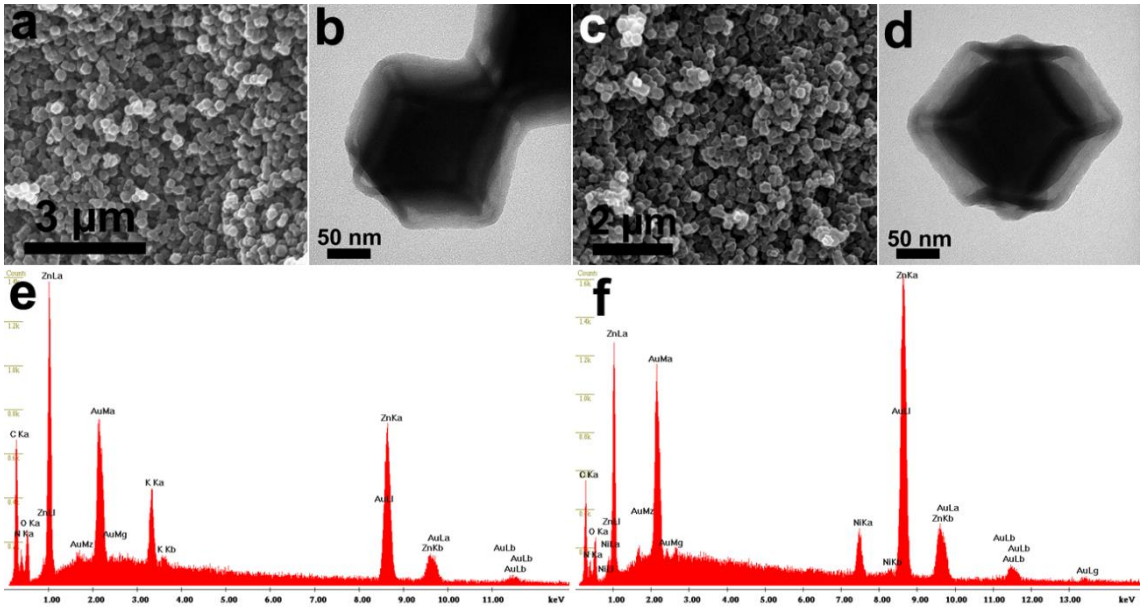

Figure S6. SEM, TEM images and EDS spectra of ZIF-8@K-TA (a, b, e) and ZIF-8@Ni-TA (c, d, f).

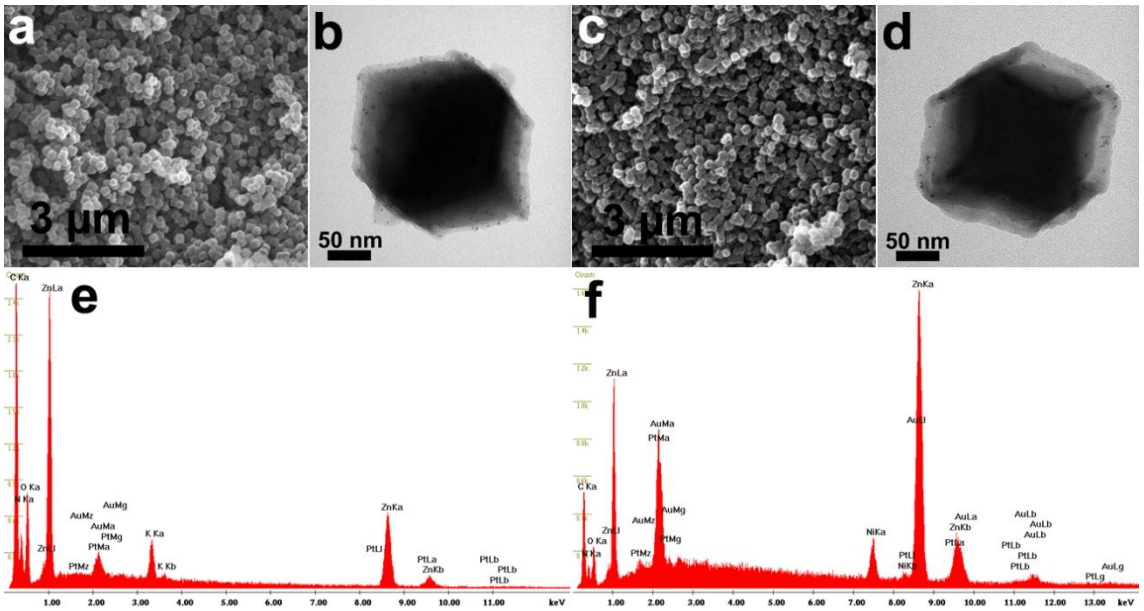

Figure S7. SEM, TEM images and EDS spectra of ZIF-8/Pt@K-TA (a, b, e) and ZIF-8/Pt@Ni-TA (c, d, f).

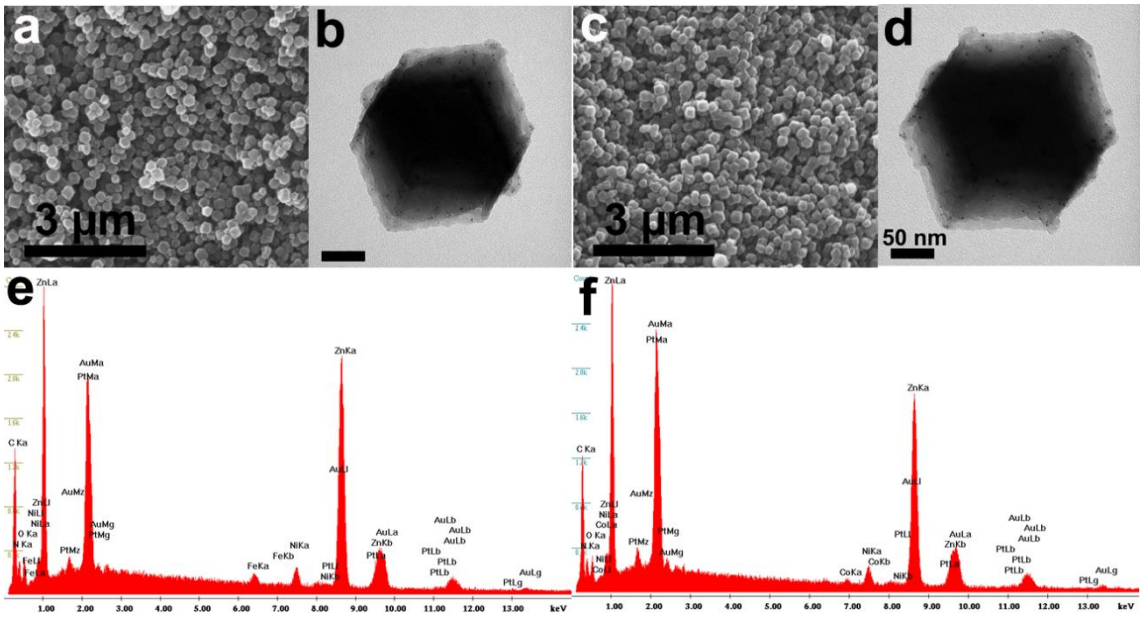

Figure S8. SEM, TEM images and EDS spectra of ZIF-8/Pt@NiFe-TA (a, b, e) and ZIF-8/Pt@NiCo-TA (c, d, f).

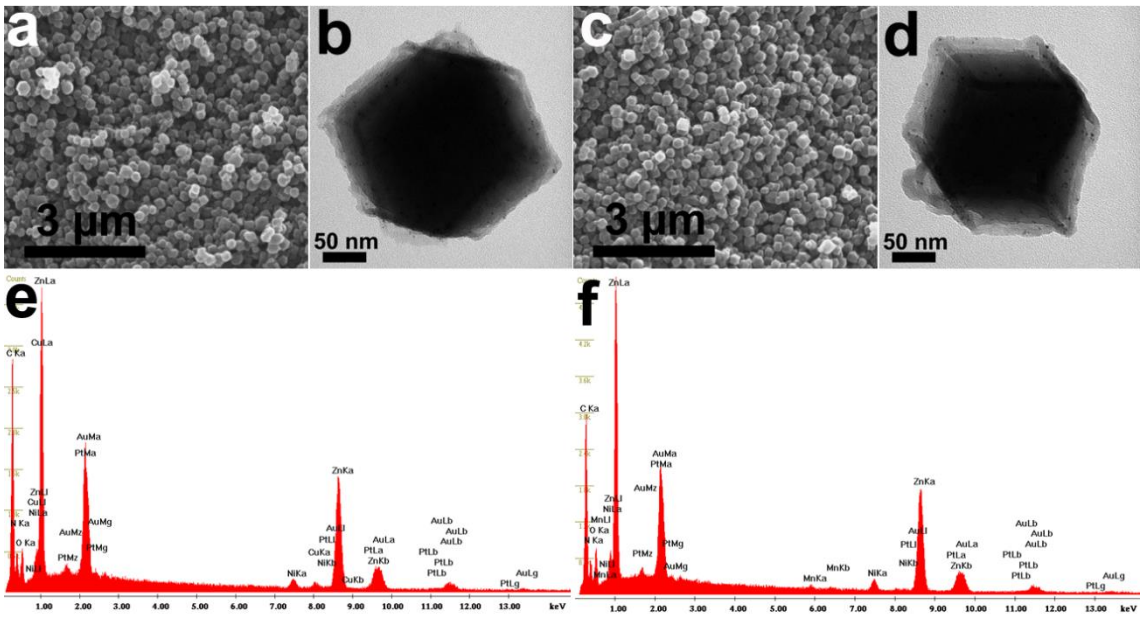

Figure S9. SEM, TEM images and EDS spectra of ZIF-8/Pt@NiCu-TA (a, b, e) and ZIF-8/Pt@NiMn -TA (c, d, f).

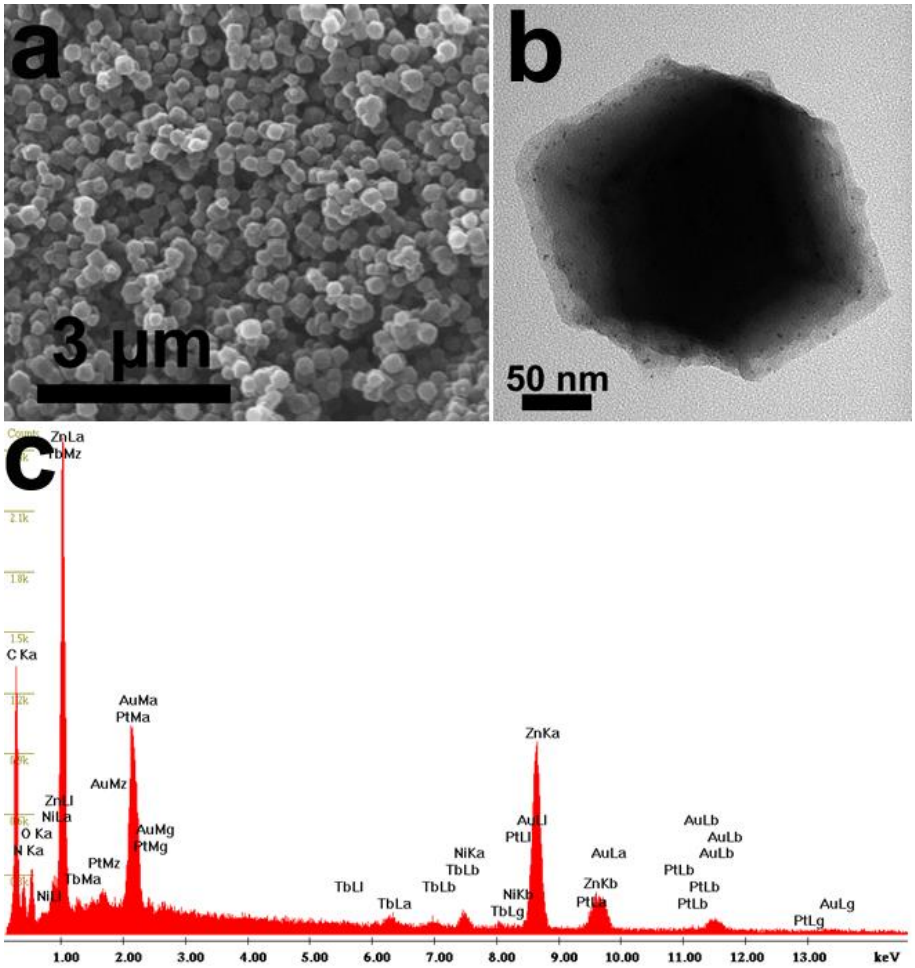

Figure S10. SEM, TEM images and EDS spectrum of ZIF-8/Pt@NiTb-TA.

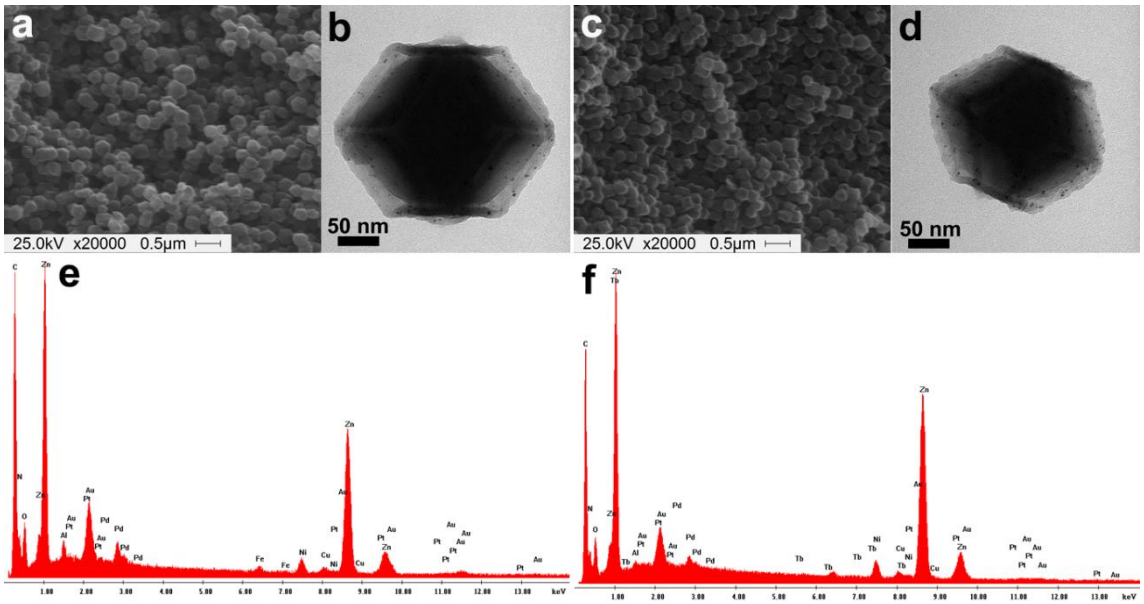

Figure S11. SEM, TEM images and EDS spectra of ZIF-8/Pt@NiCuFe-TA (a, b, e) and ZIF-8/Pt@NiCuTb -TA (c, d, f).

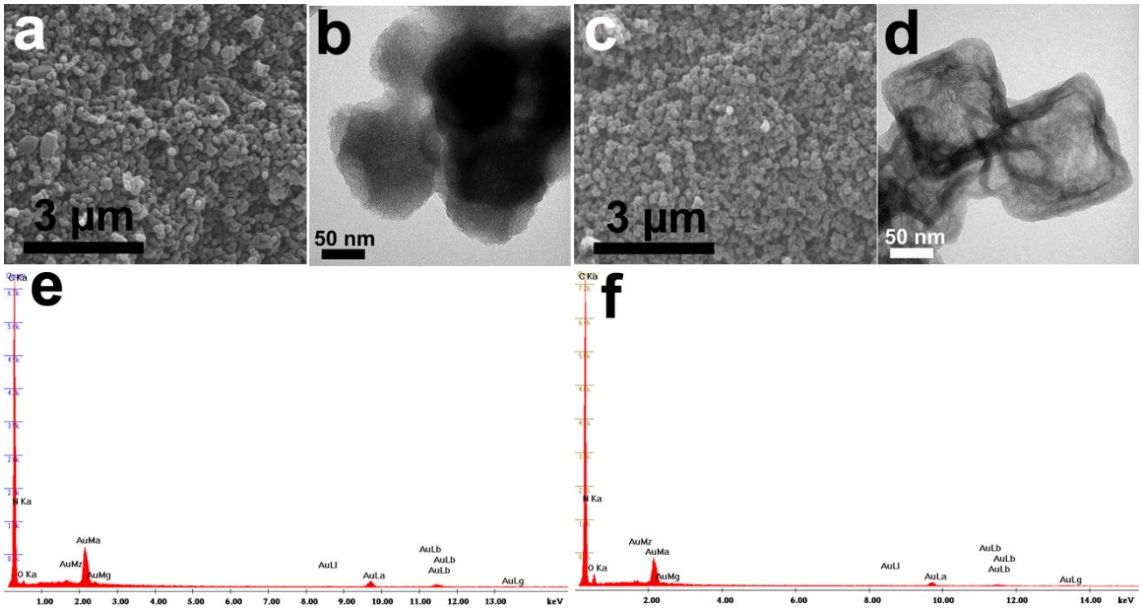

Figure S12. SEM, TEM images and EDS spectra of NC (a, b, e) and NPCC (c, d, f).

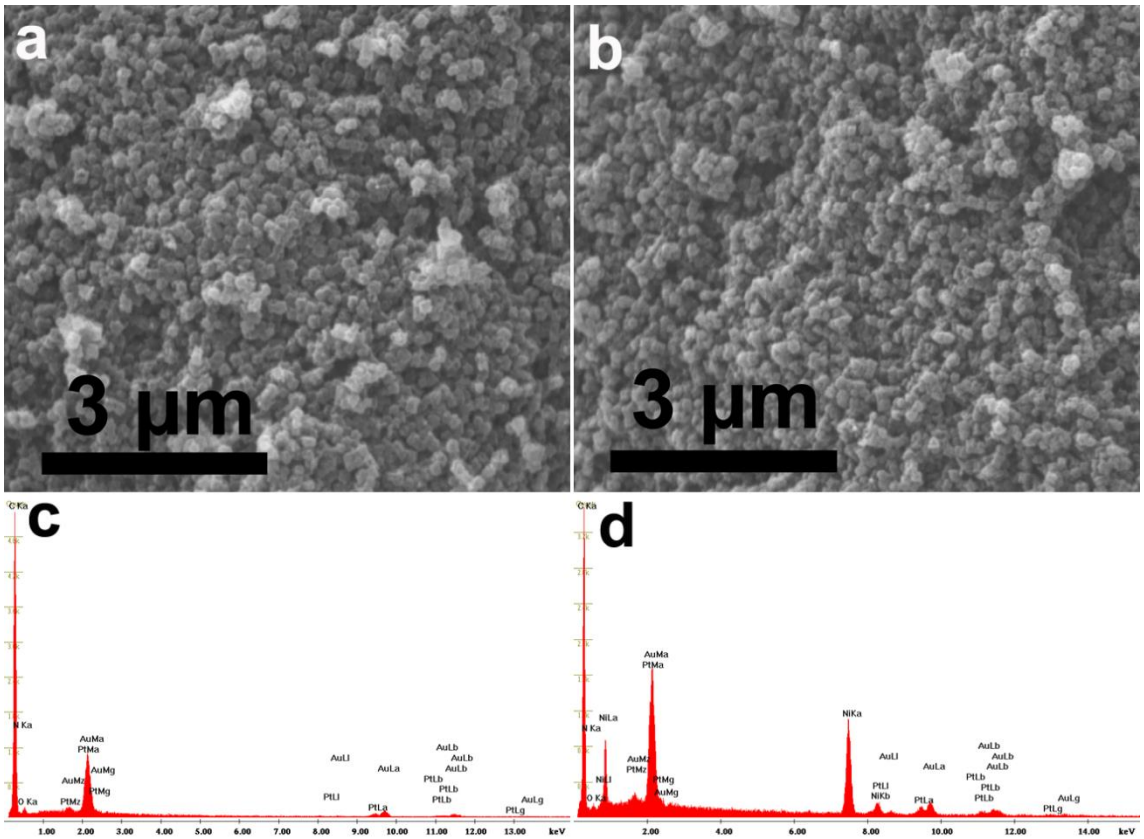

Figure S13. SEM images and EDS spectra of Pt@NPCC (a, c) and PtNi@NPCC (b, d).

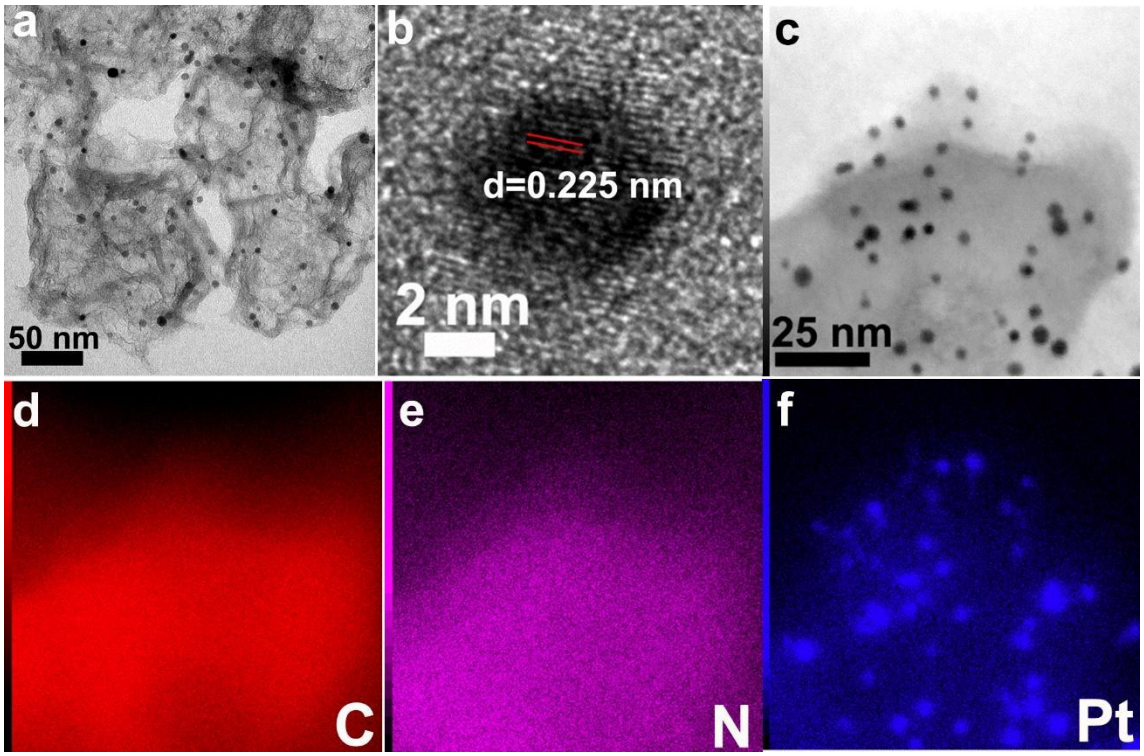

Figure S14. (a)TEM image of Pt@NPCC. (b) HRTEM image of an individual Pt nanoparticle. (c-f) STEM image and elemental mapping of Pt@NPCC.

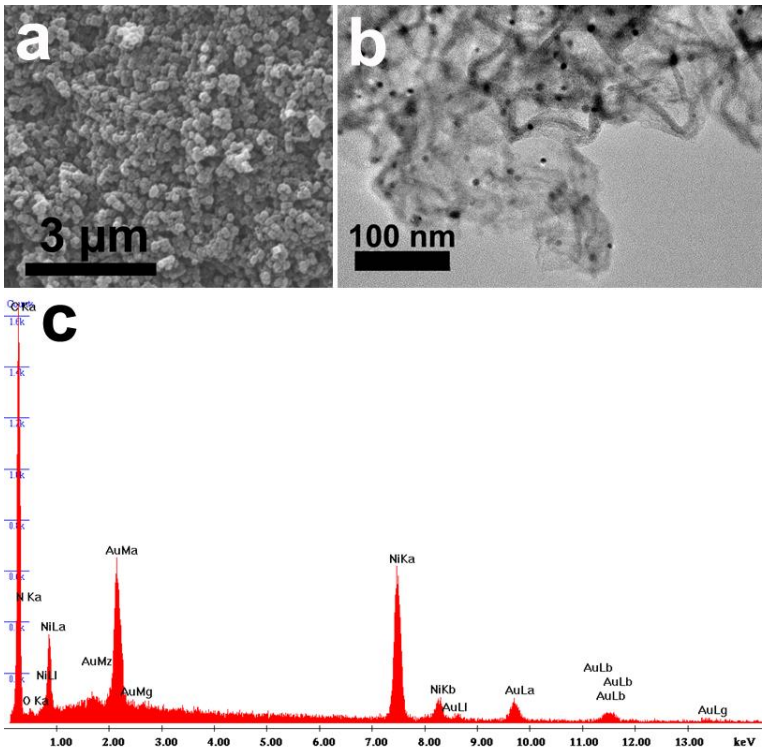

Figure S15. SEM, TEM images and EDS spectrum of Ni@NPCC.

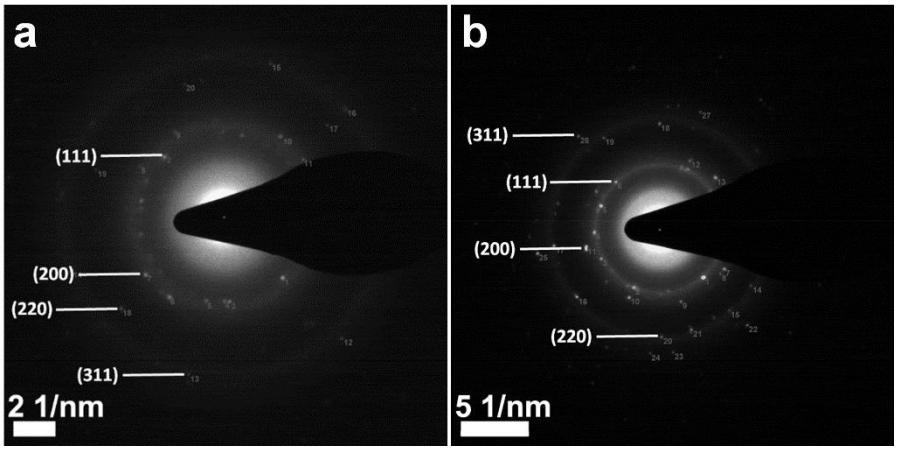

Figure S16. SAED of (a) Pt@NPCC, and (b) Ni@NPCC. Diffractions peaks corresponding to lattice planes of PtNPs and NiNPs, respectively, are highlighted.

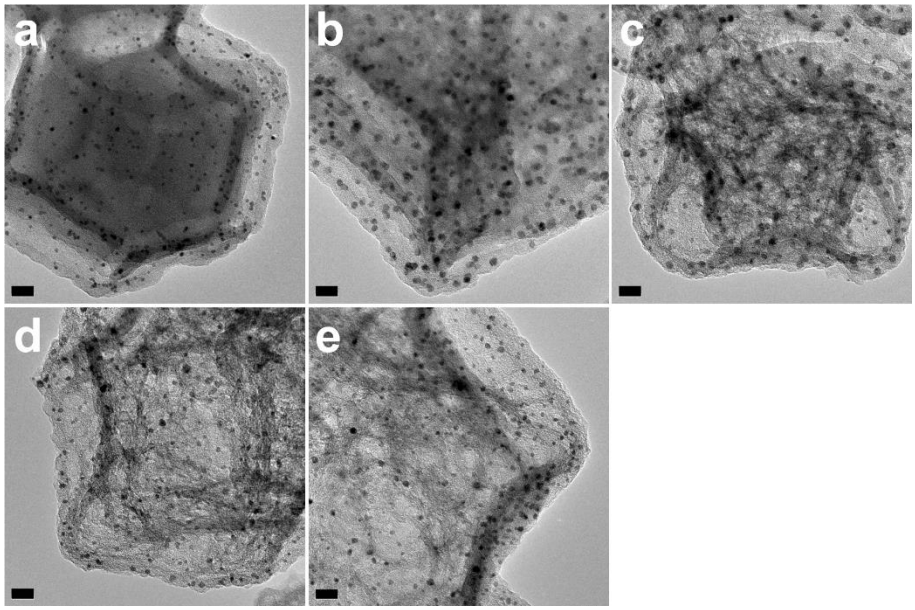

Figure S17. TEM images of ZIF-8/Pt@Ni-TA calcined at (a) 500 °C, (b) 600 °C, (c) 700 °C, (d) 800 °C, and (e) 900 °C. The scale bars represent 20 nm.

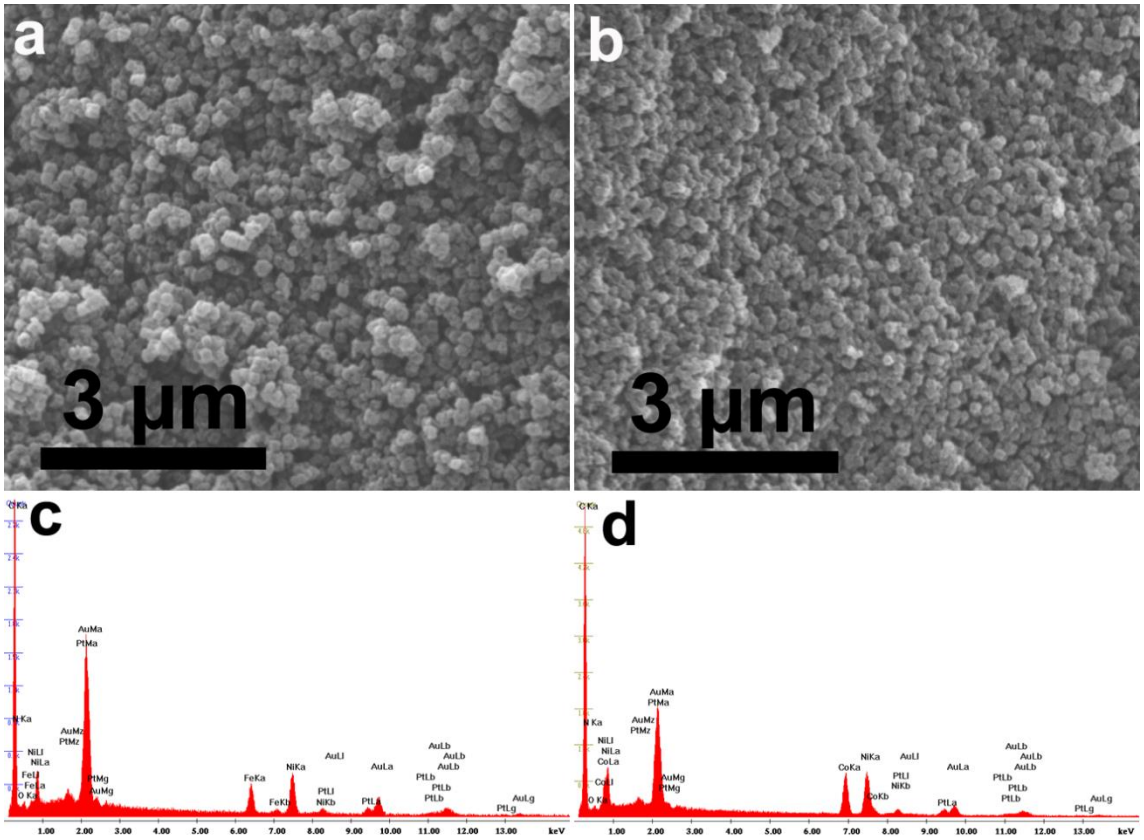

Figure S18. SEM images and EDS spectra of PtNiFe@NPCC (a, c) and PtNiCo@NPCC (b, d).

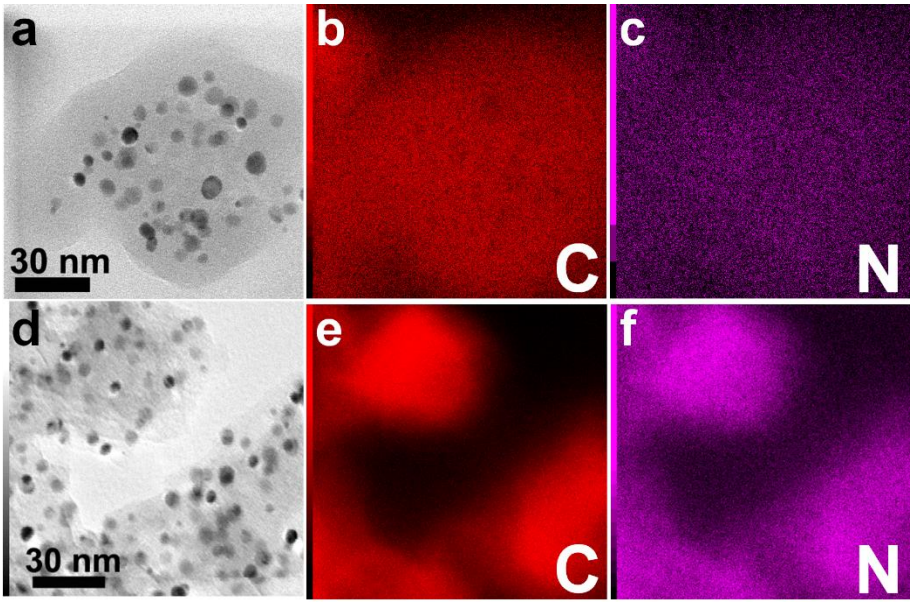

Figure S19. STEM images and elemental mapping of PtNiFe@NPCC (a, b, c) and PtNiCo@NPCC (d, e, f).

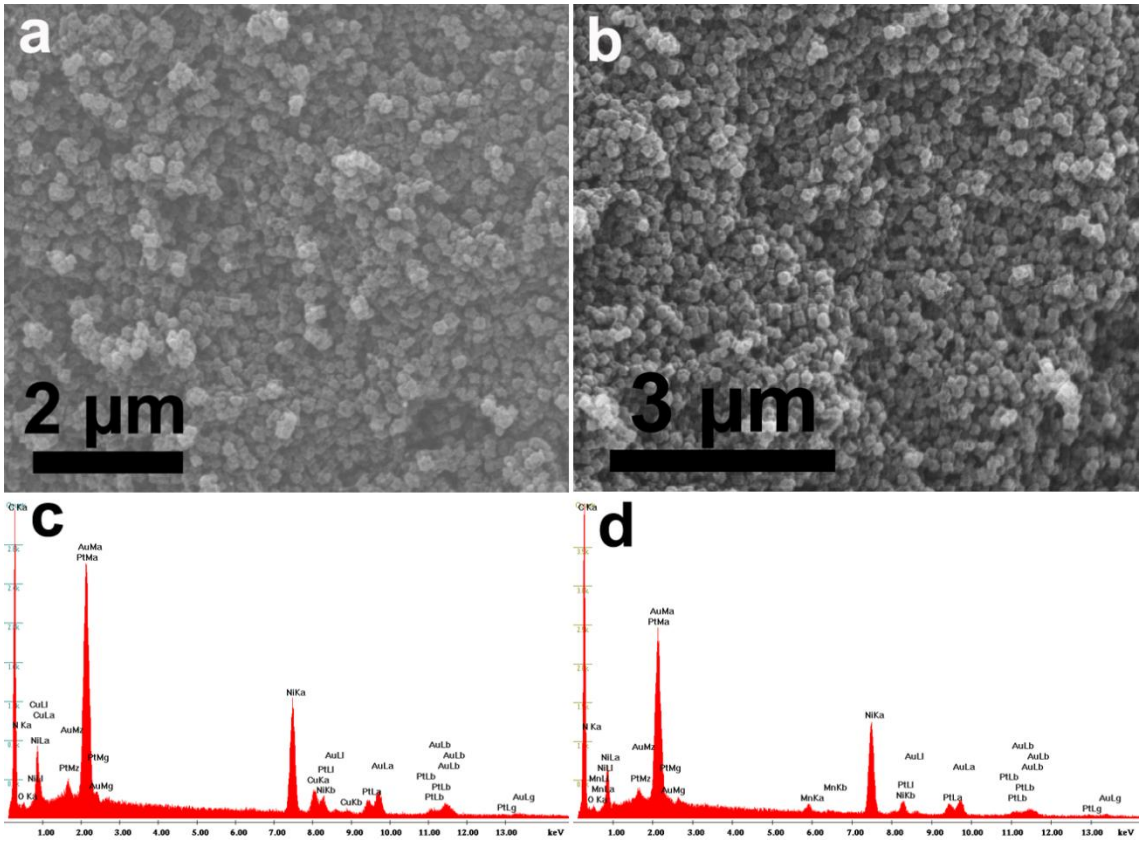

Figure S20. SEM images and EDS spectra of PtNiCu@NPCC (a, c) and PtNiMn@NPCC (b, d).

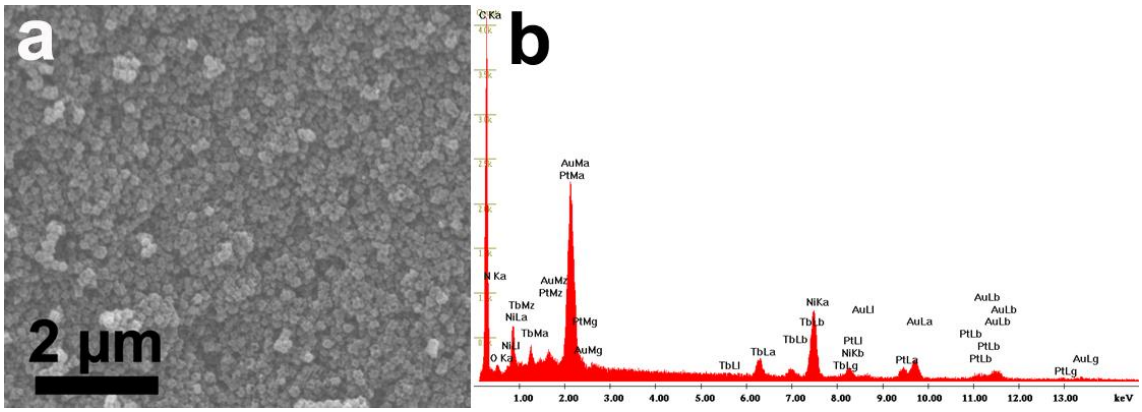

Figure S21. SEM image and EDS spectrum of PtNiTb@NPCC.

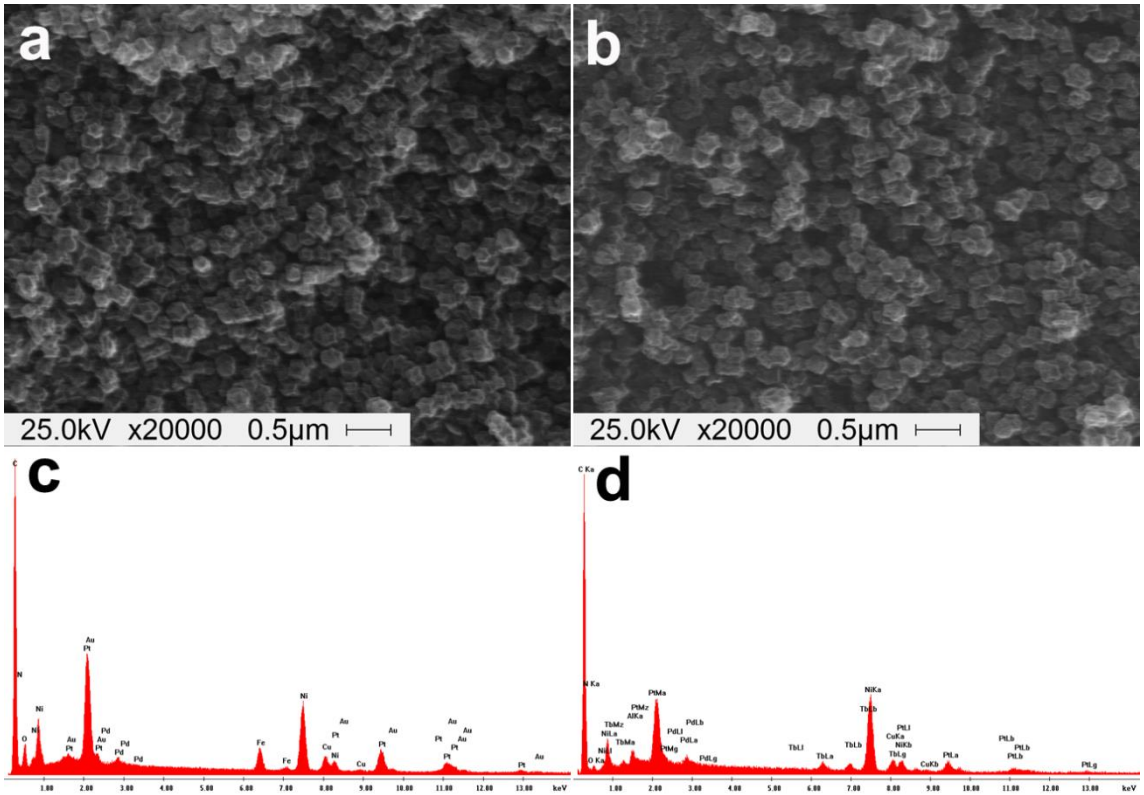

Figure S22. SEM images and EDS spectra of PtNiCuFe@NPCC (a, c) and PtNiCuTb@NPCC (b, d).

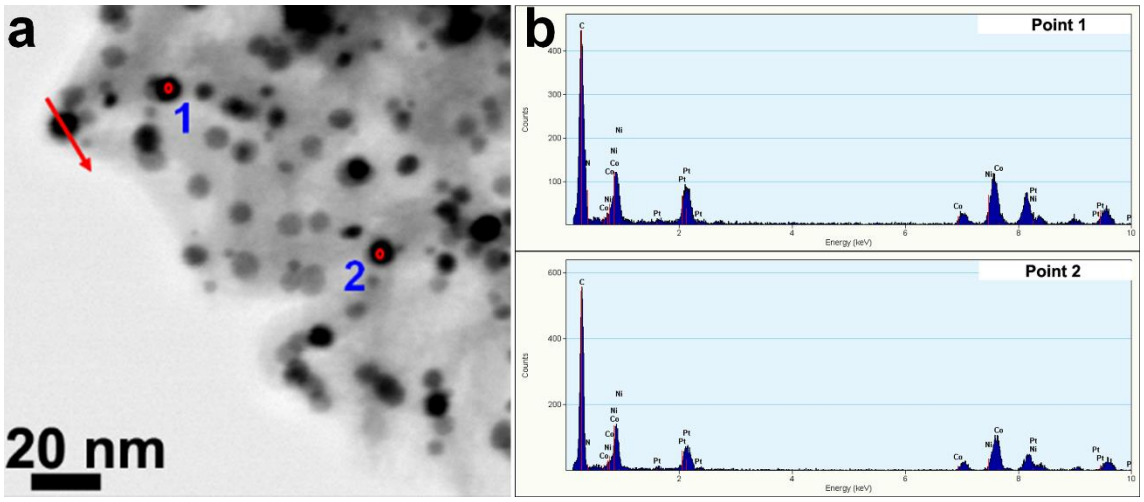

Figure S23. (a) STEM image of PtNiCo@NPCC. (b) EDS spectra of point 1 and point 2 on **a**.

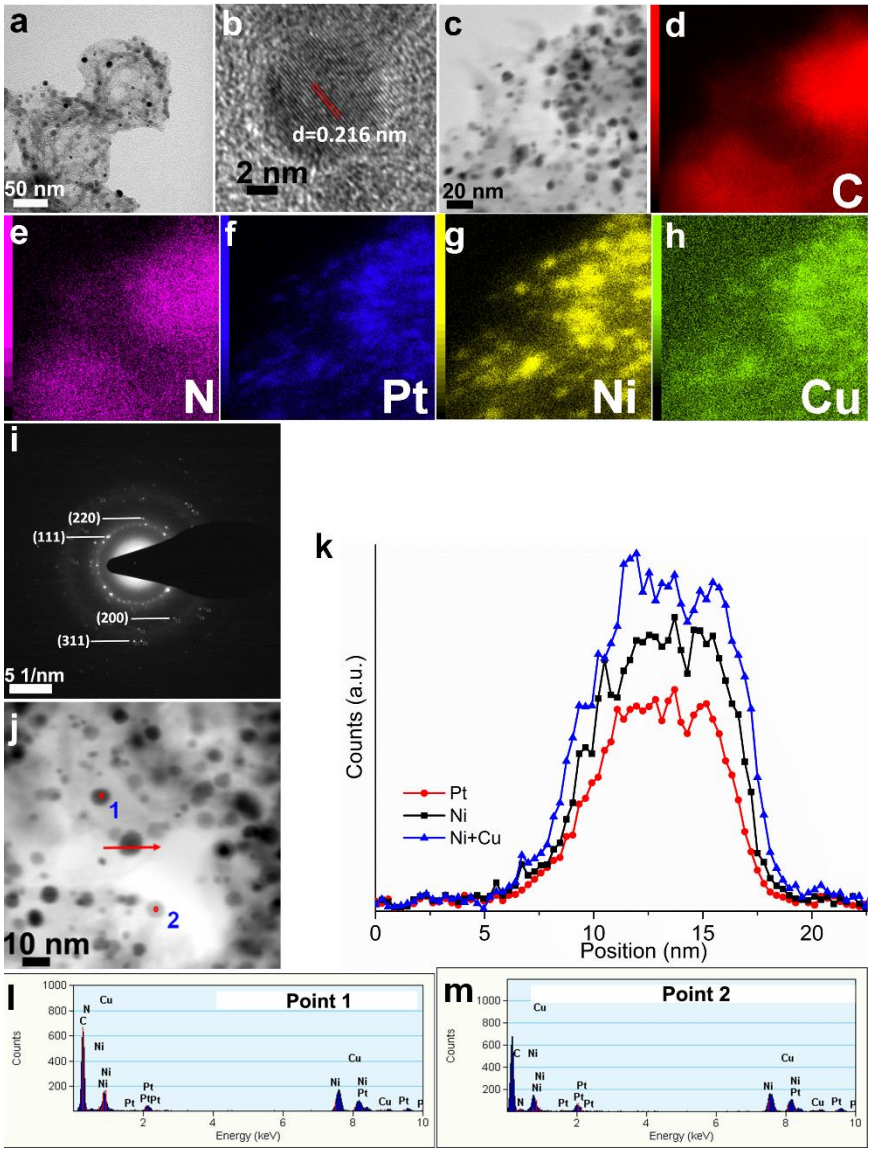

Figure S24. (a) TEM image of PtNiCu@NPCC. (b) HRTEM image showing an individual PtNiCu trimetallic nanoparticle. (c-h) STEM image and elemental mapping of PtNiCu@NPCC. (i) SAED of PtNiCu@NPCC. STEM image (j) and linear distributions of Pt, Ni and Cu along the arrow line on **j** (k). (l, m) EDS spectra of point 1 and point 2 on **j**.

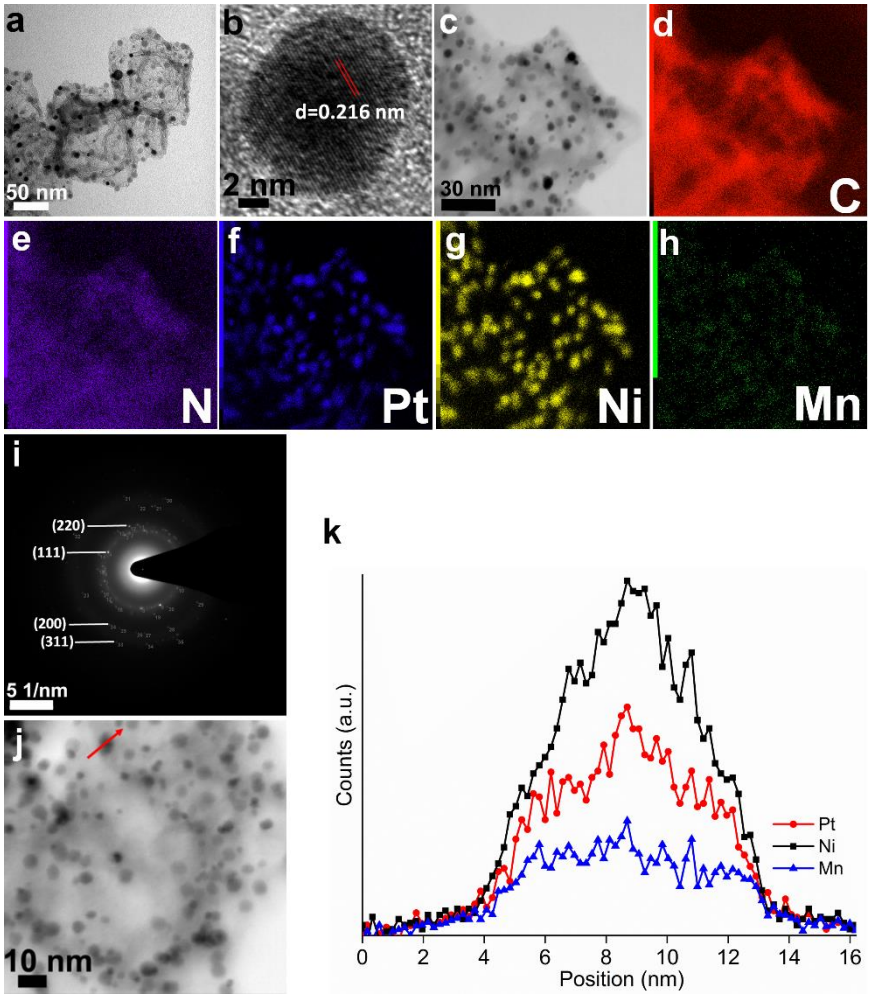

Figure S25. (a) TEM image of PtNiMn@NPCC. (b) HRTEM image showing an individual PtNiMn trimetallic nanoparticle. (c-h) STEM image and elemental mapping of PtNiMn@NPCC. (i) SAED of PtNiMn@NPCC. STEM image (j) and linear distributions of Pt, Ni and Mn along the arrow line on **j** (k).

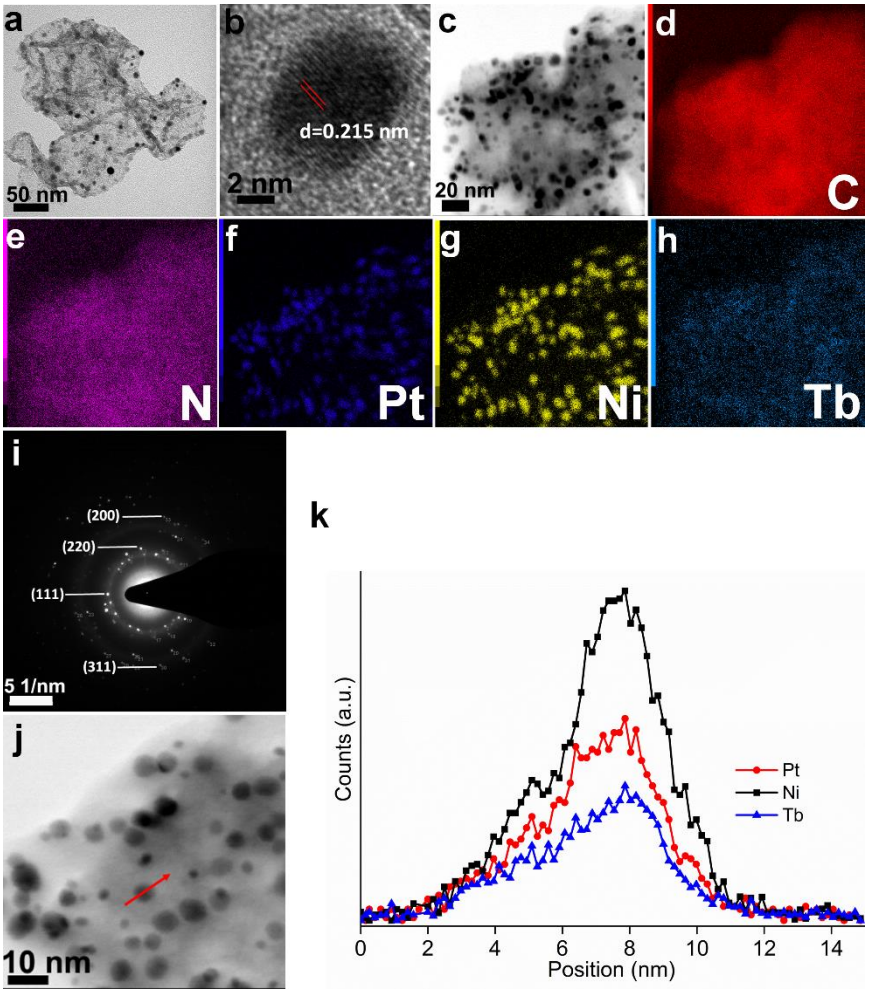

Figure S26. (a) TEM image of PtNiTb@NPCC. (b) HRTEM image showing an individual PtNiTb trimetallic nanoparticle. (c-h) STEM image and elemental mapping of PtNiTb@NPCC. (i) SAED of PtNiTb@NPCC. STEM image (j) and linear distributions of Pt, Ni and Tb along the arrow line on **j** (k).

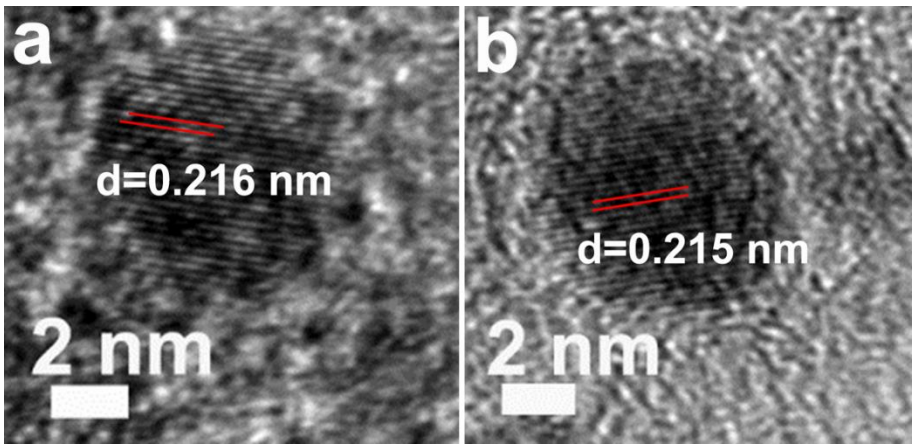

Figure S27. HRTEM images of PtNiCuFe@NPCC (a) and PtNiCuTb@NPCC (b).

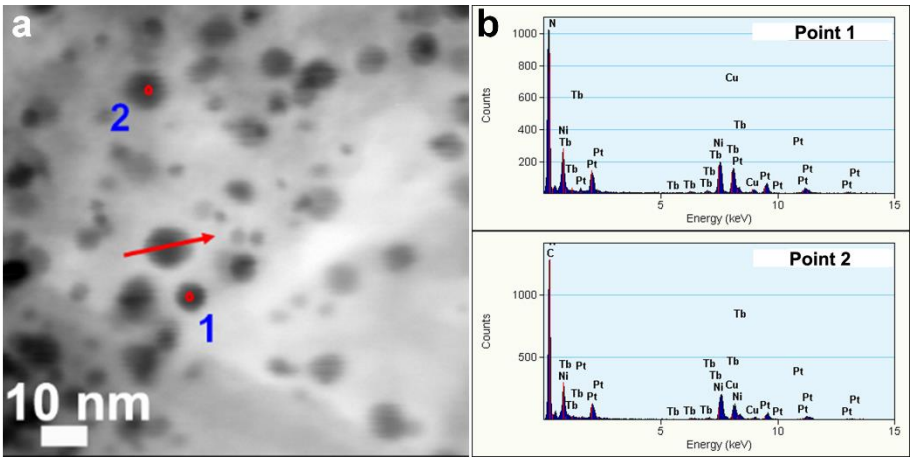

Figure S28. (a) STEM image of PtNiCuTb@NPCC. (b) EDS spectra of point 1 and point 2 on **a**.

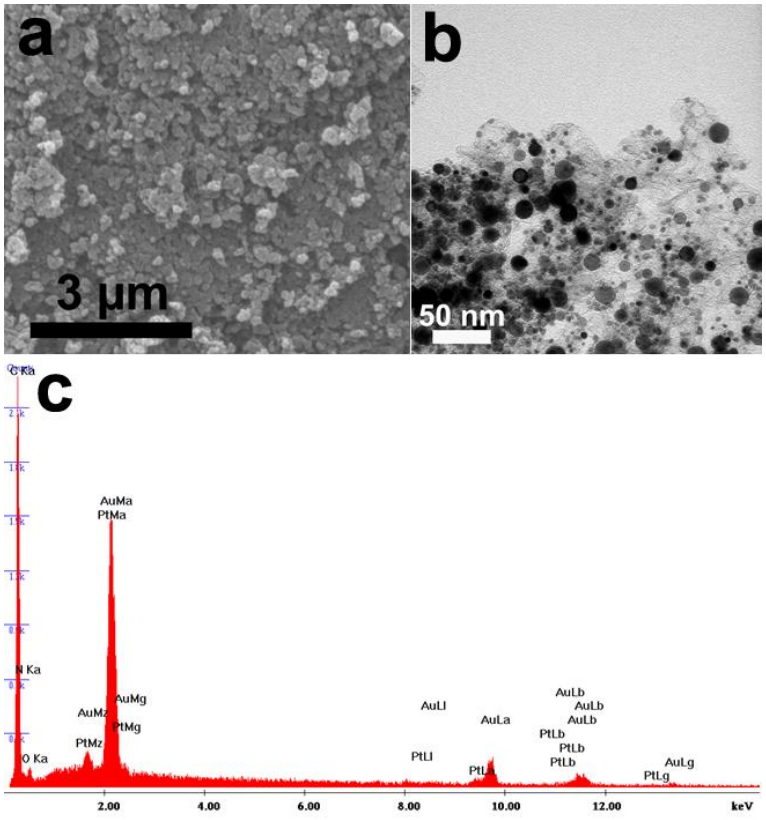

Figure S29. SEM, TEM images and EDS spectrum of Pt/NC.

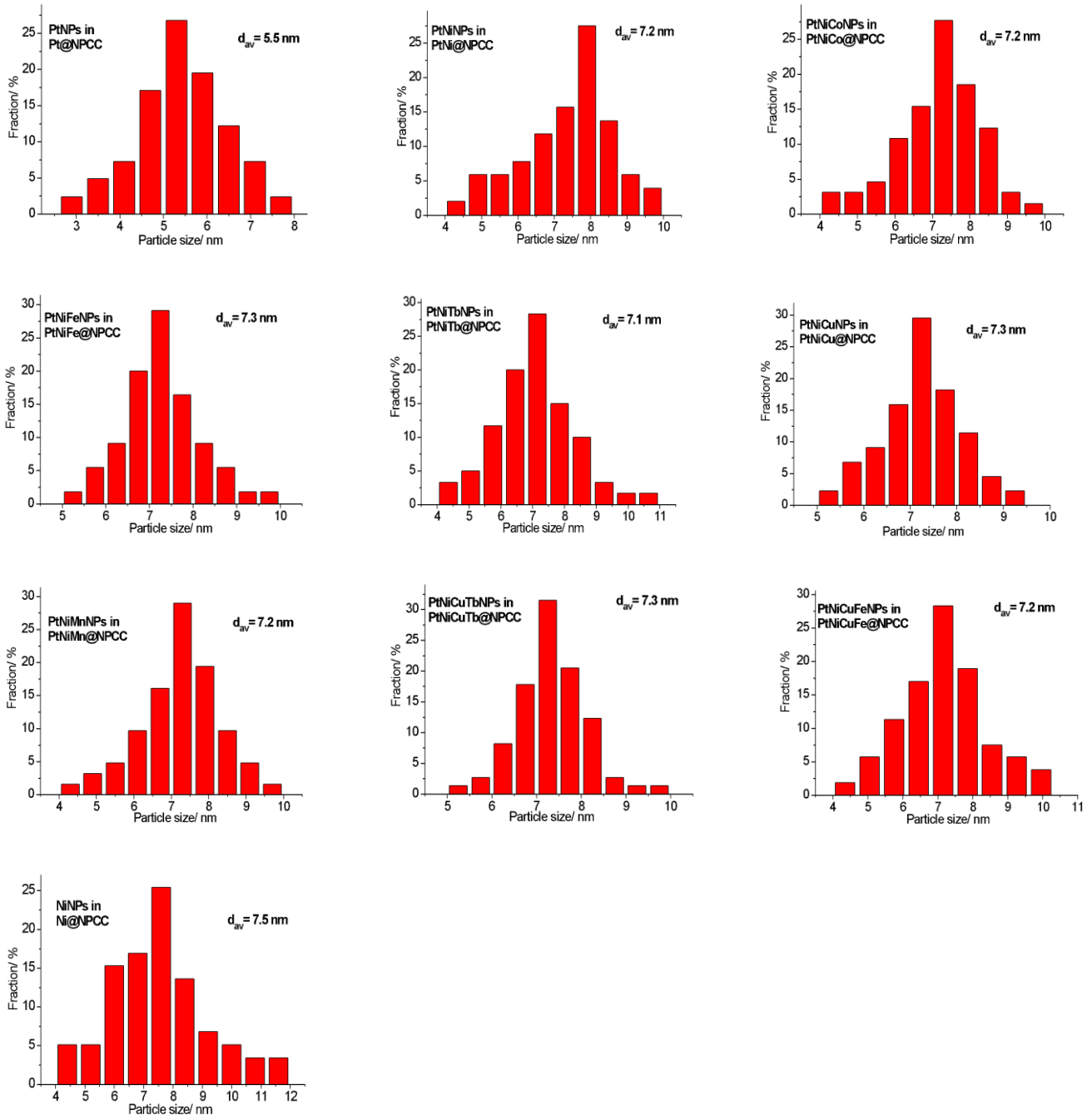

Figure S30. Histograms of nanoparticle size and average particle sizes for each material.

4.4 Nitrogen adsorption measurements, pore size analysis and surface area calculations:

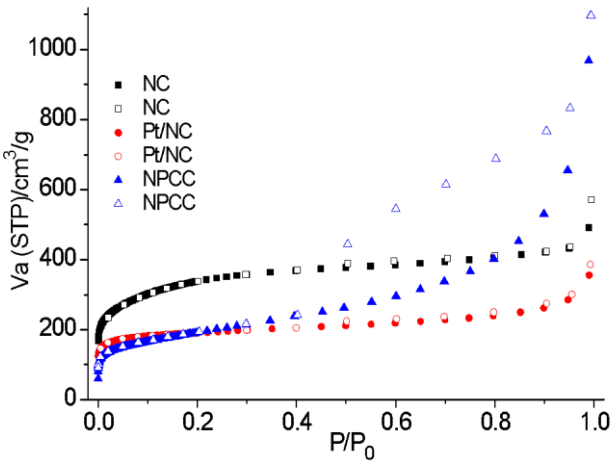

Figure S31. N_2 adsorption (filled symbols) and desorption (open symbols) isotherms measured at 77 K.

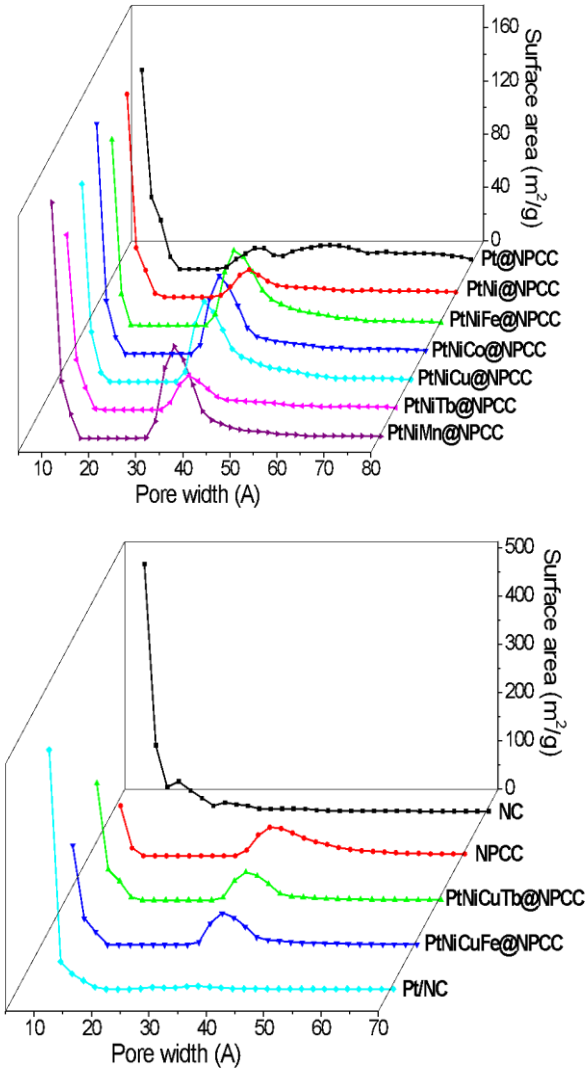

Figure S32. Pore size distribution plots calculated using a DFT method from N_2 isotherms measured at 77 K.

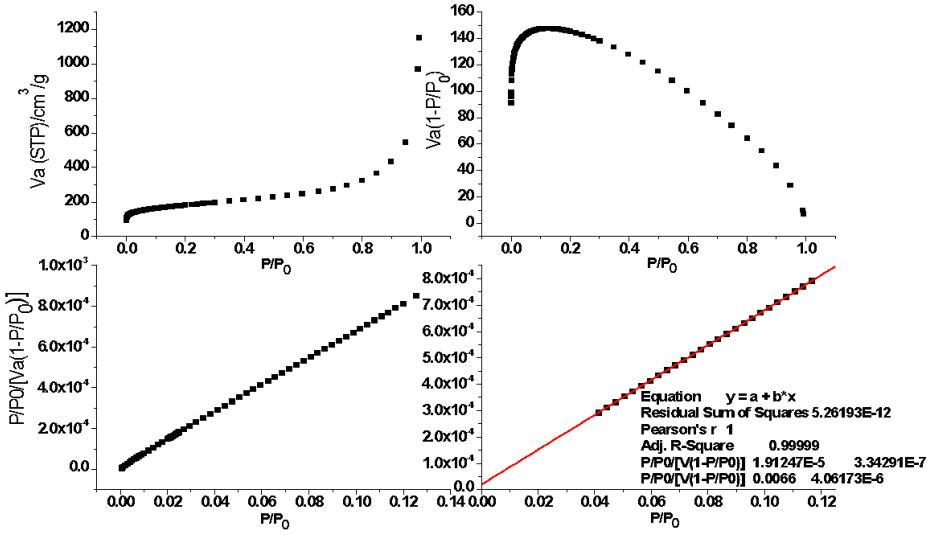

Figure S33. Top left: N_2 adsorption isotherm for PtNiFe@NPCC at 77 K. Top right: Consistency plot for the N_2 isotherm in PtNiFe@NPCC. Bottom left: Plot $P/P_0/[v(1-P/P_0)]$ against P/P_0 for the N_2 isotherm of PtNiFe@NPCC. Bottom right: BET equation plot for PtNiFe@NPCC.

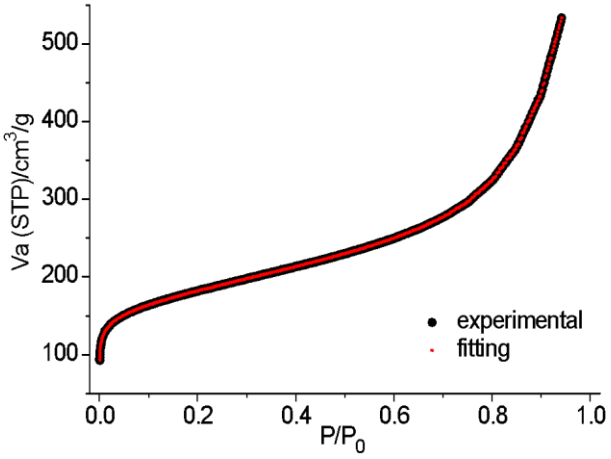

Figure S34. N_2 adsorption isotherm for PtNiFe@NPCC at 77 K (black). Fitting comparison by QSDFT model (red).

4.5 Fourier Transform Infrared Spectroscopy (FT-IR)

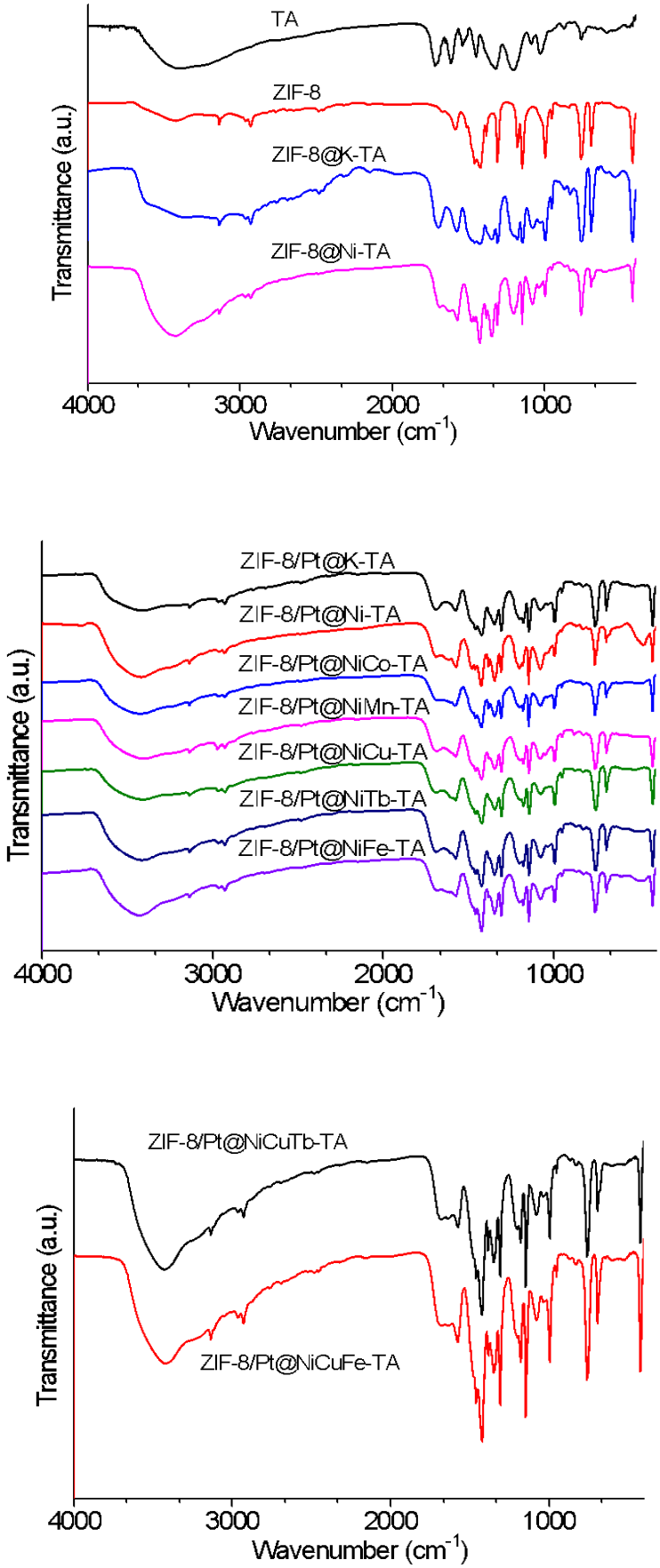

Figure S35. FTIR spectra of each material.

4.6 Raman Spectroscopy

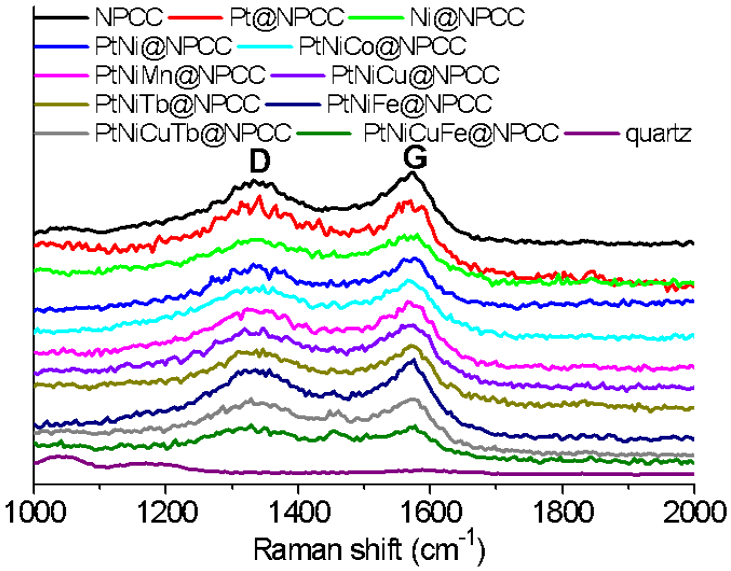

Figure S36. Raman spectra of each material.

4.7 X-ray Photoelectron Spectroscopy (XPS)

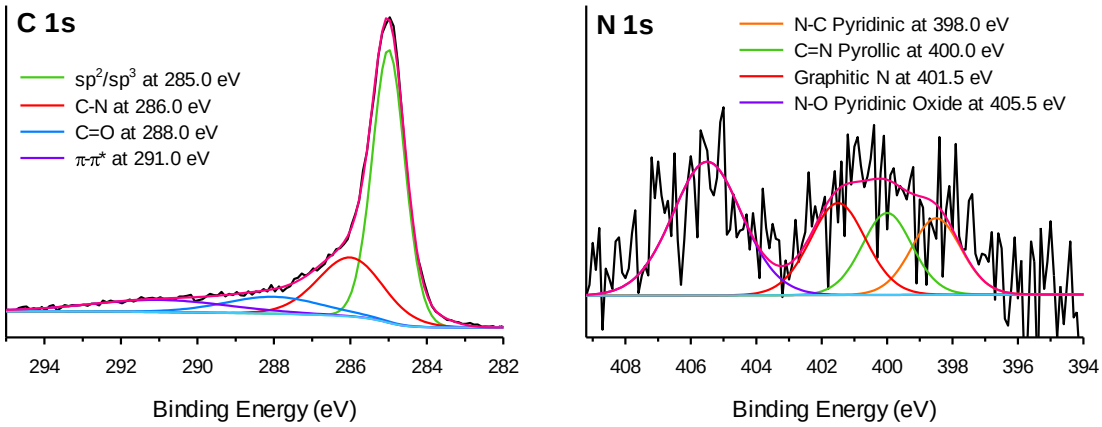

Figure S37. XPS spectra of NPCC.

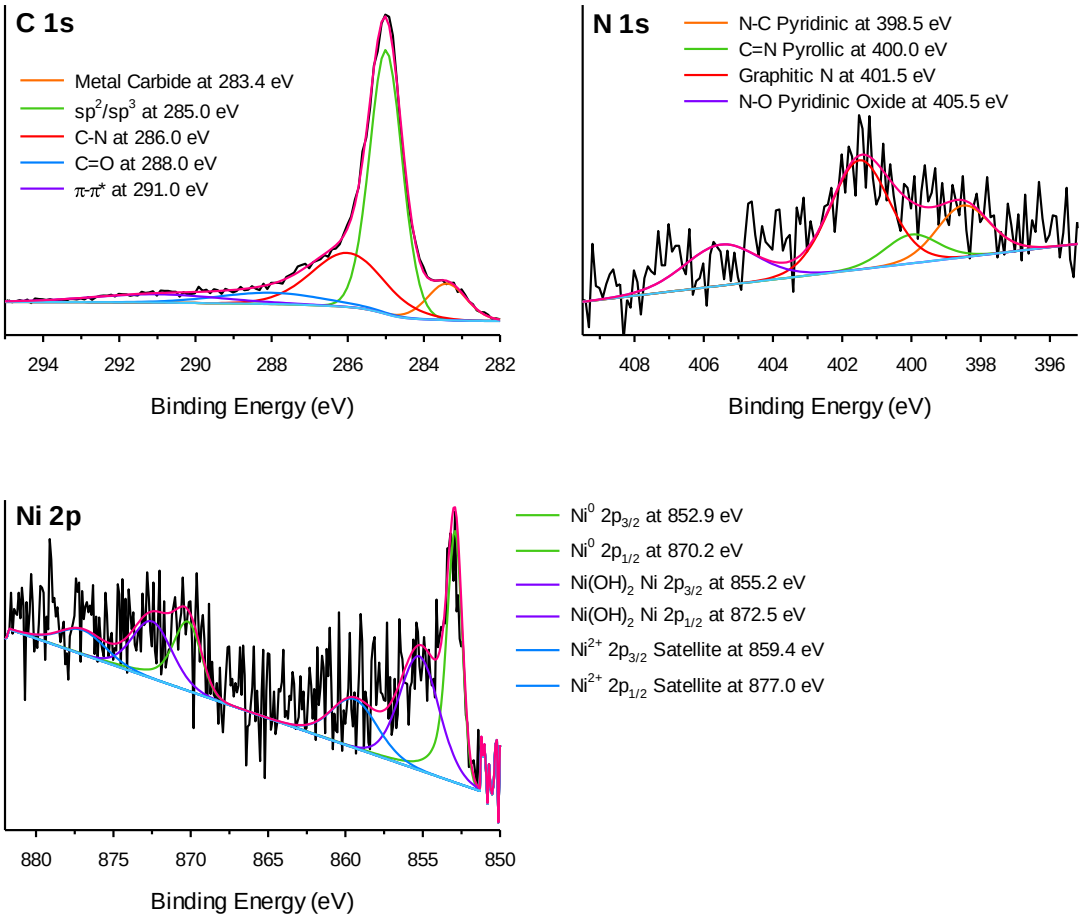

Figure S38. XPS spectra of Ni@NPCC.

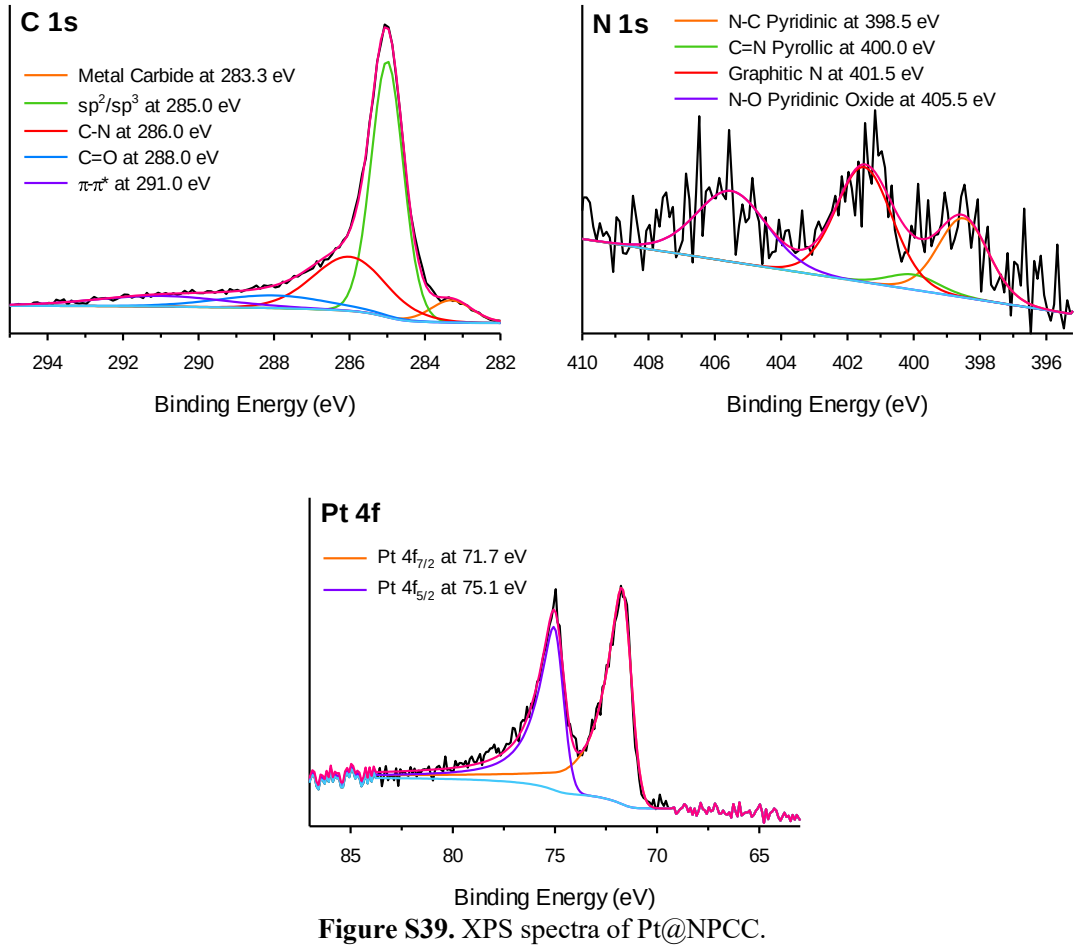

Figure S39. XPS spectra of Pt@NPCC.

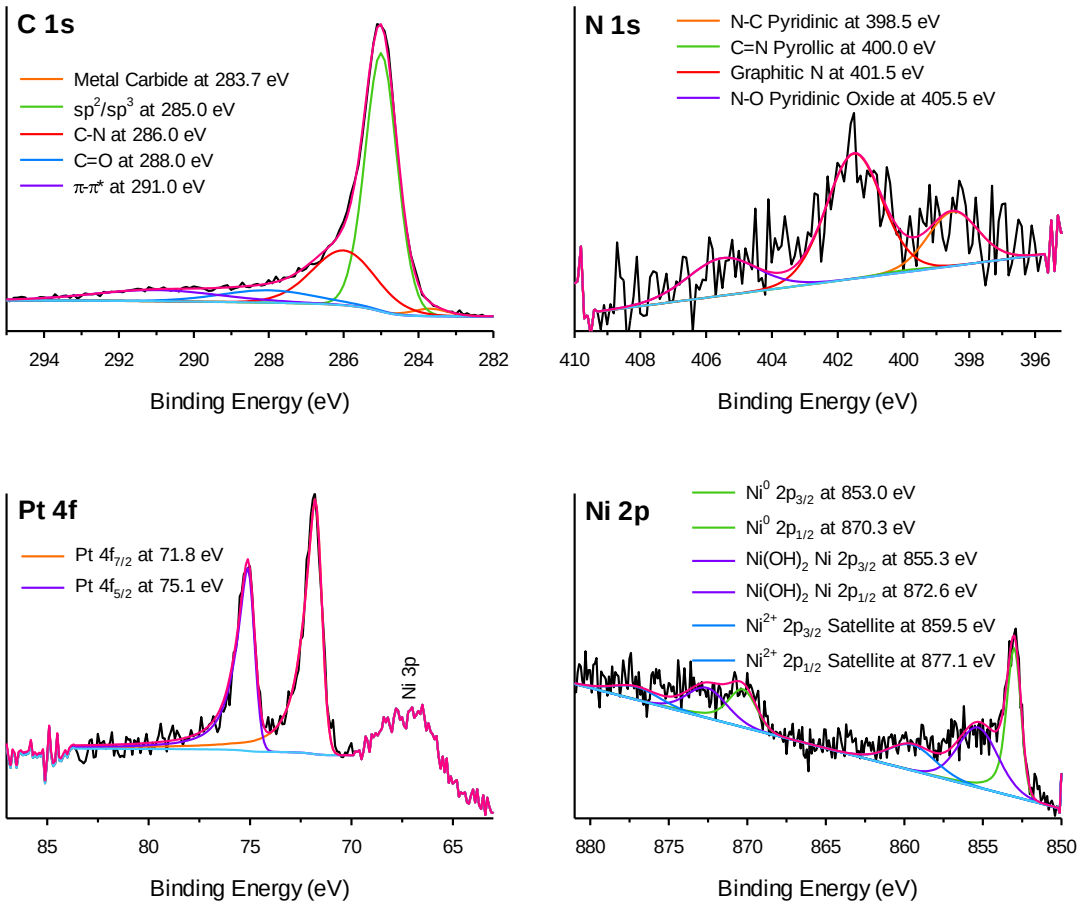

Figure S40. XPS spectra of PtNi@NPCC.

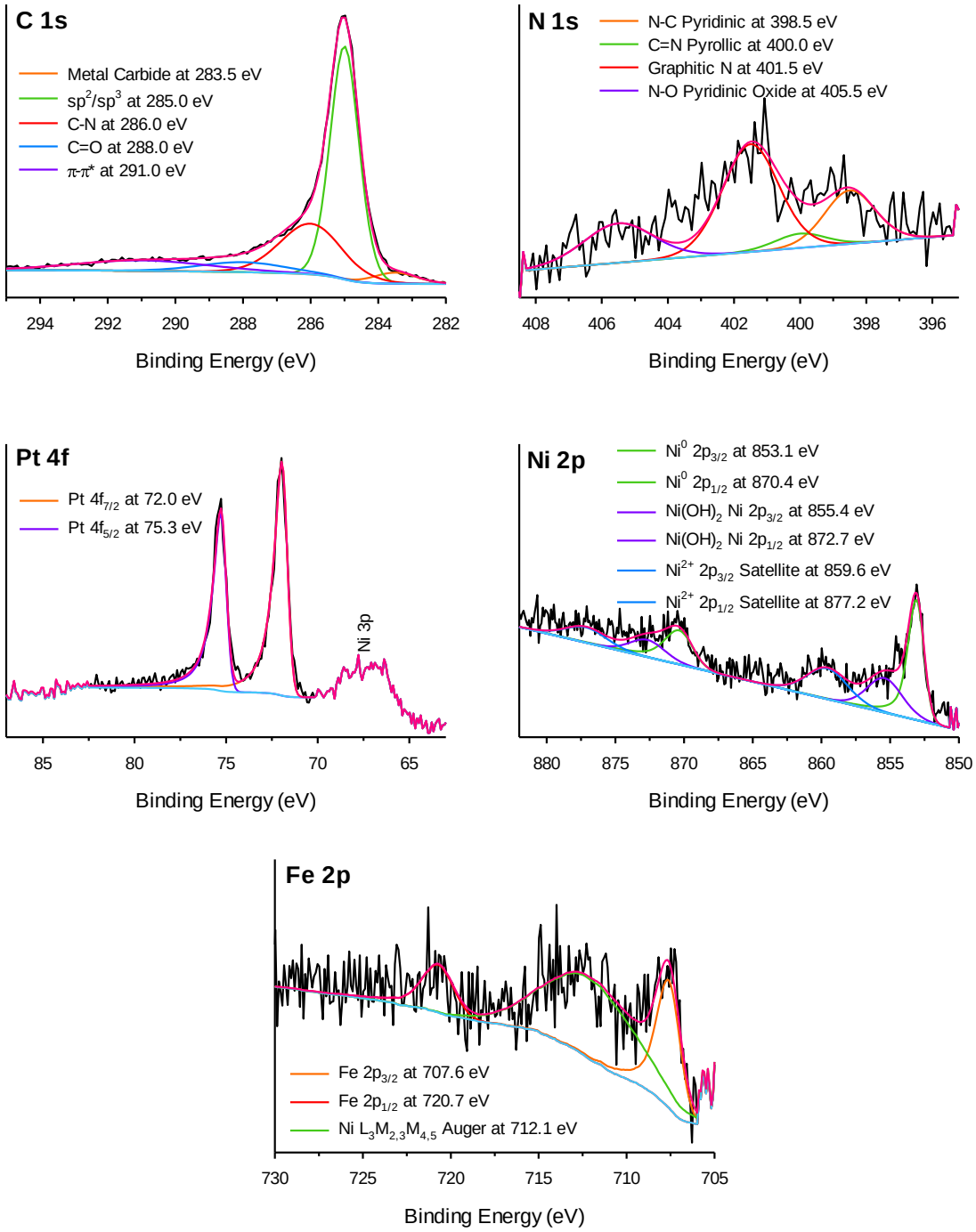

Figure S41. XPS spectra of PtNiFe@NPCC.

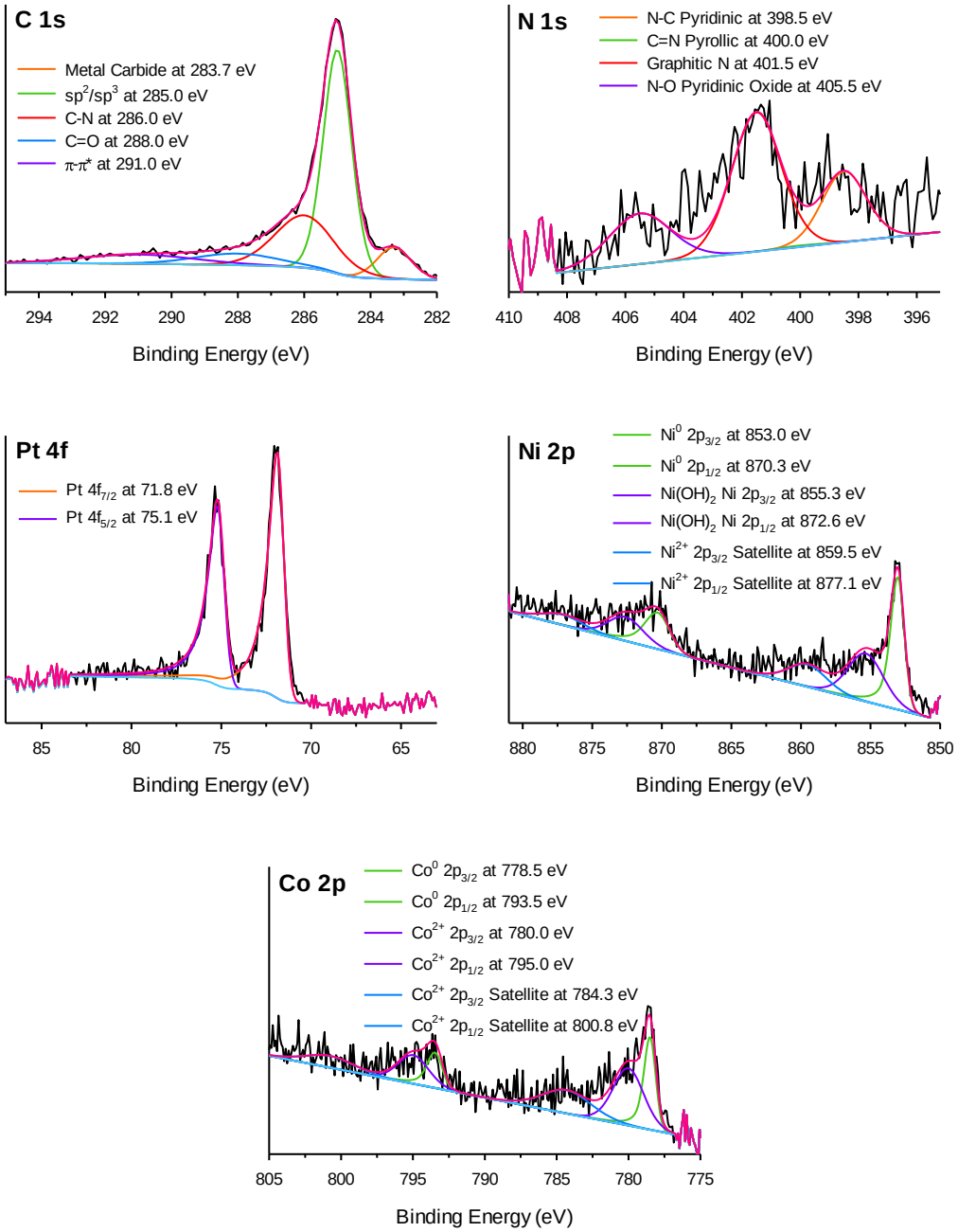

Figure S42. XPS spectra of PtNiCo@NPCC.

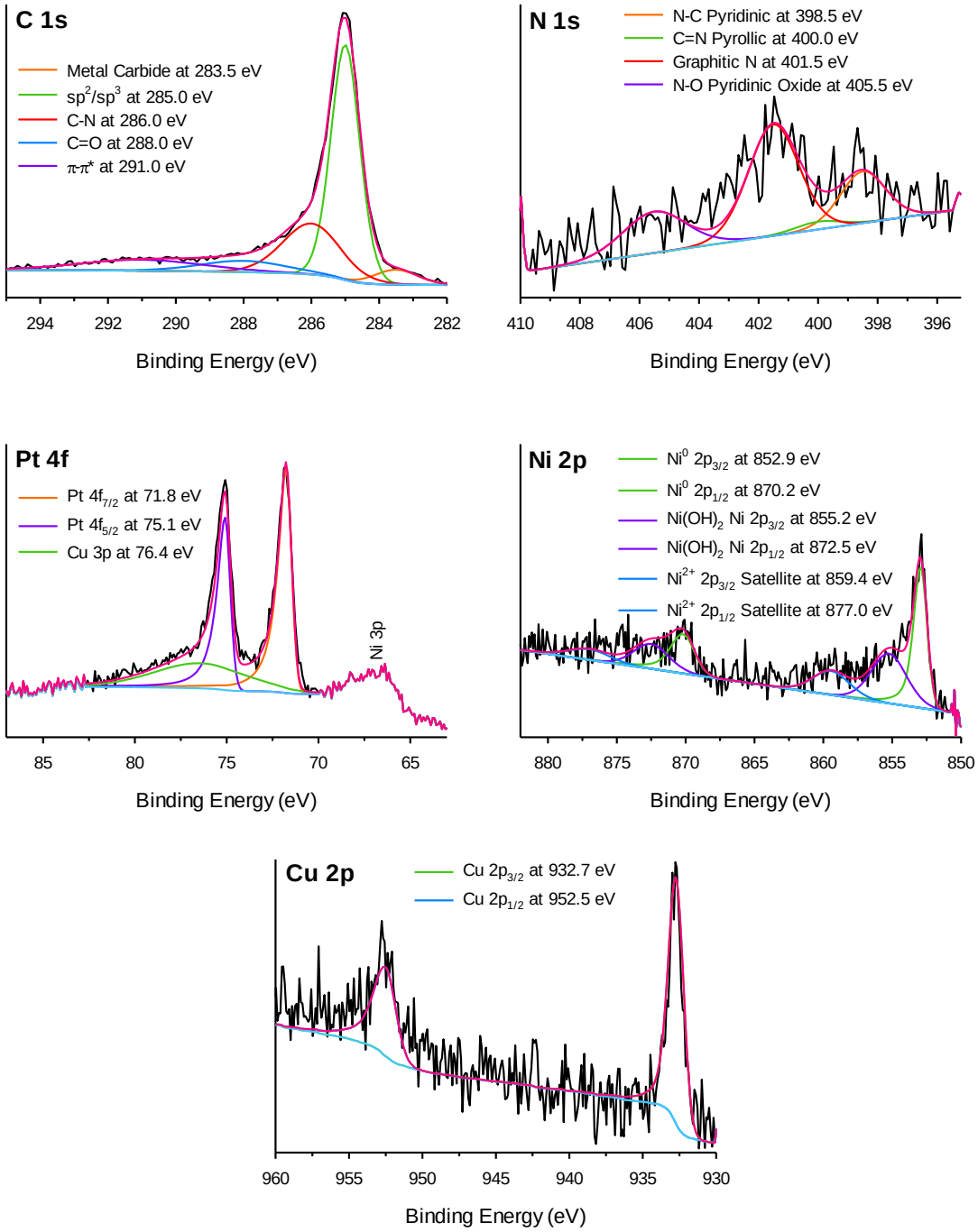

Figure S43. XPS spectra of PtNiCu@NPCC.

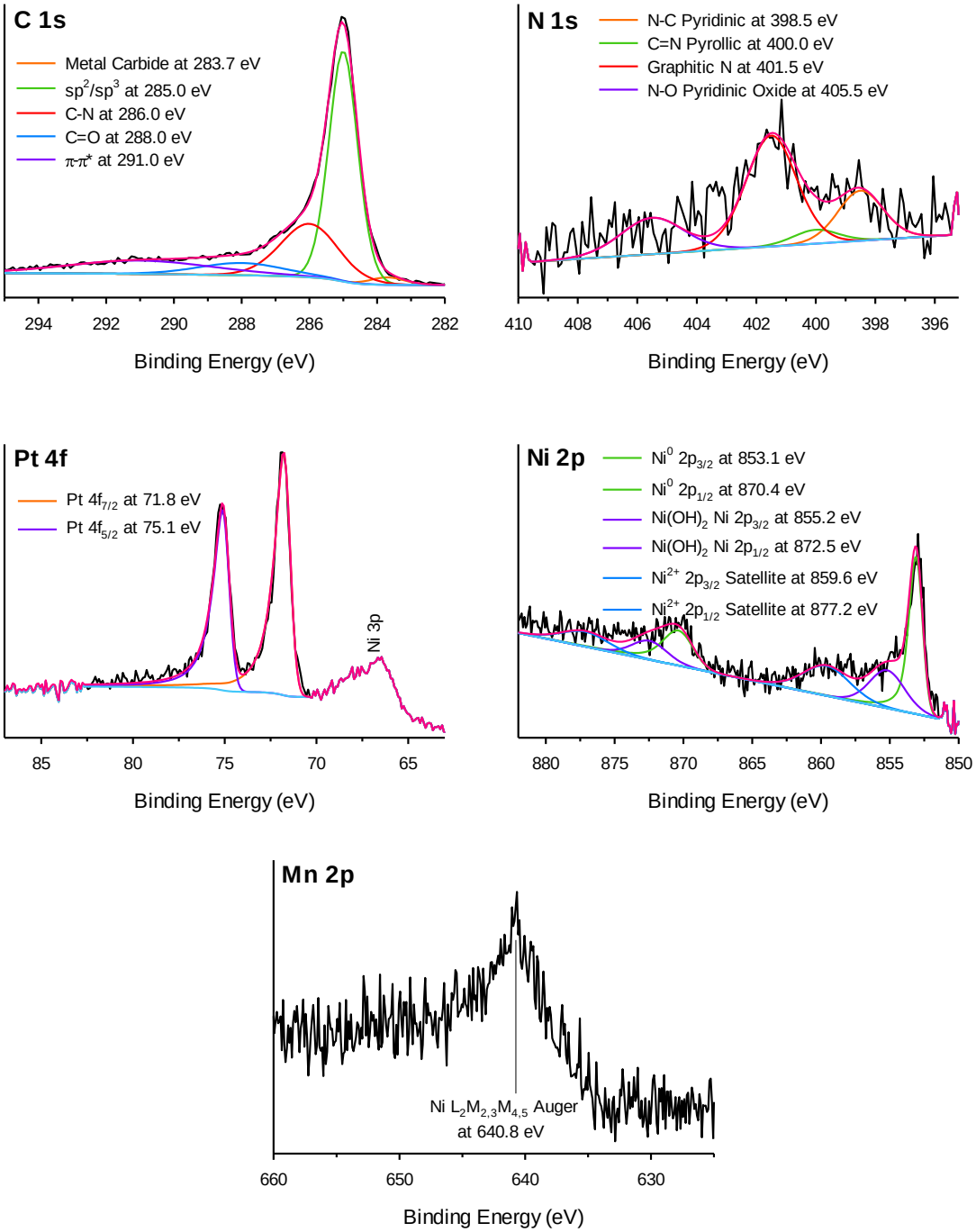

Figure S44. XPS spectra of PtNiMn@NPCC.

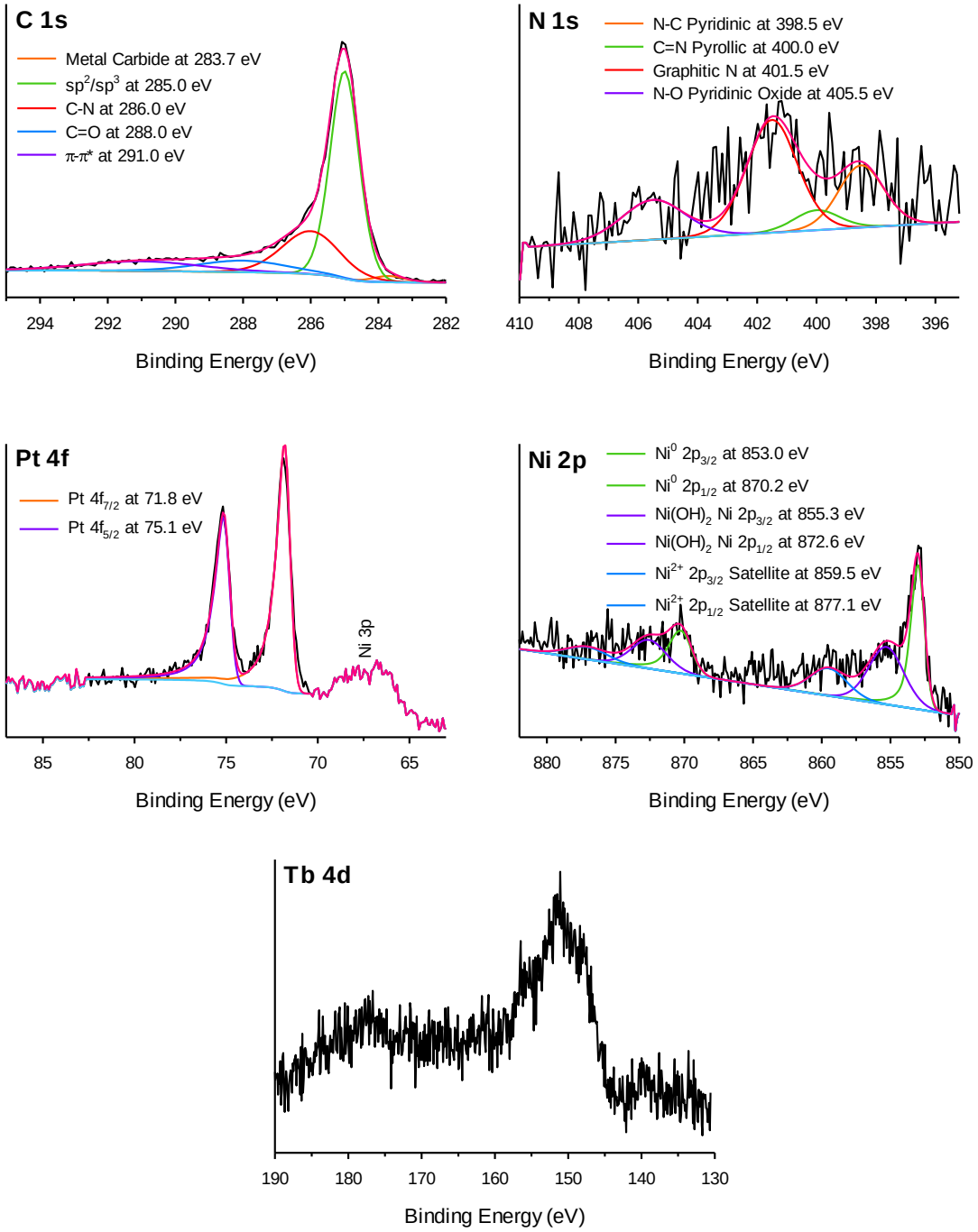

Figure S45. XPS spectra of PtNiTb@NPCC.

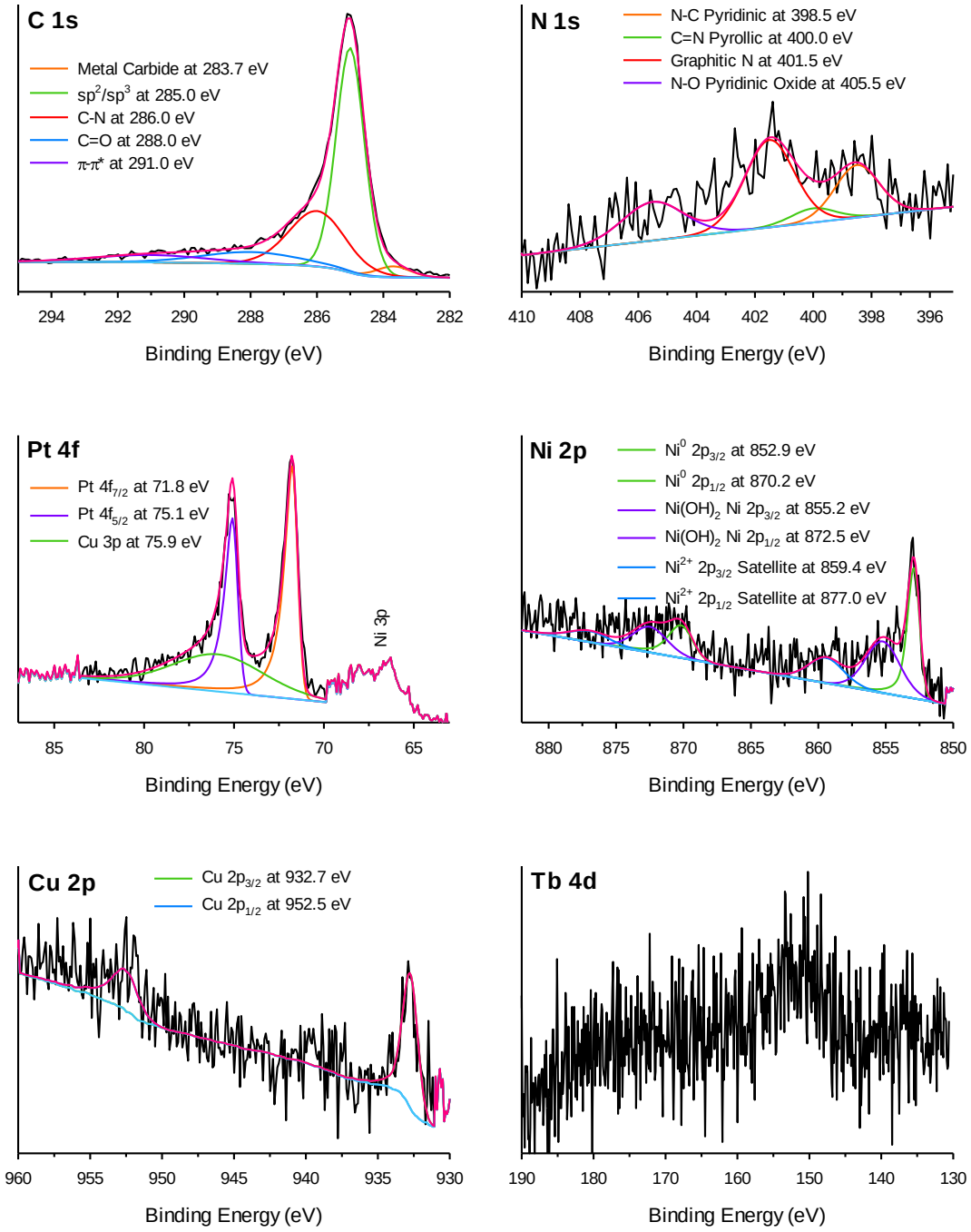

Figure S46. XPS spectra of PtNiCuTb@NPCC.

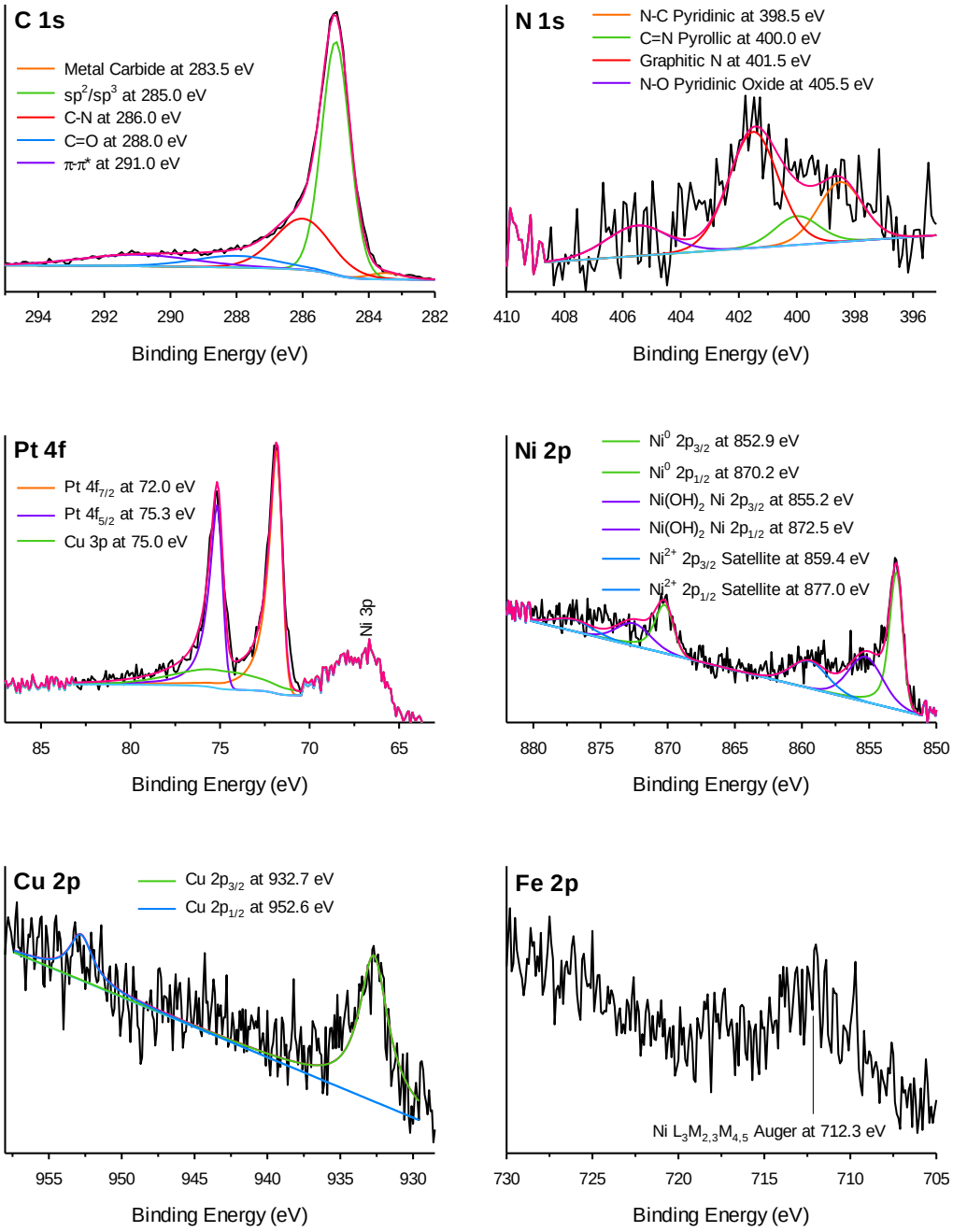

Figure S47. XPS spectra of PtNiCuFe@NPCC.

4.8 Hydrogen Evolution Reaction (HER)

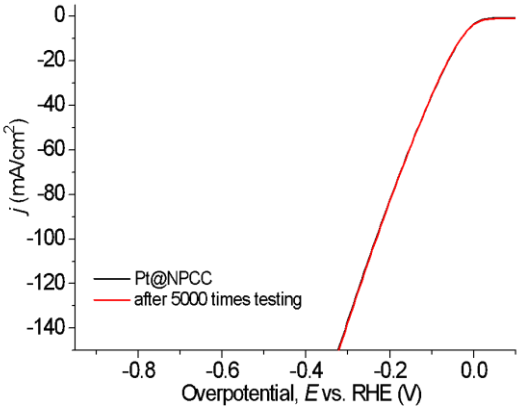

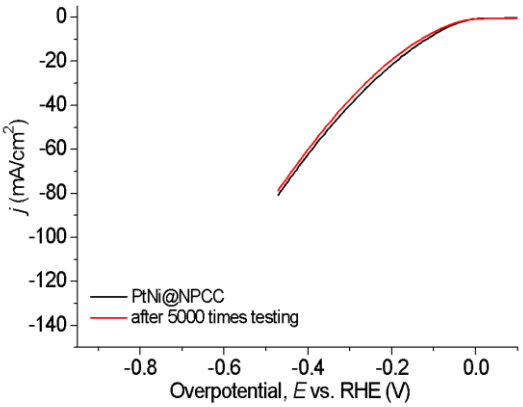

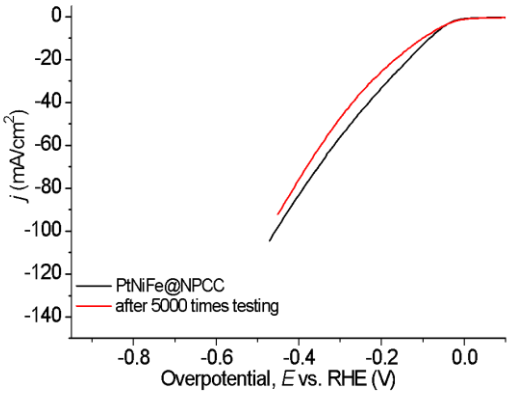

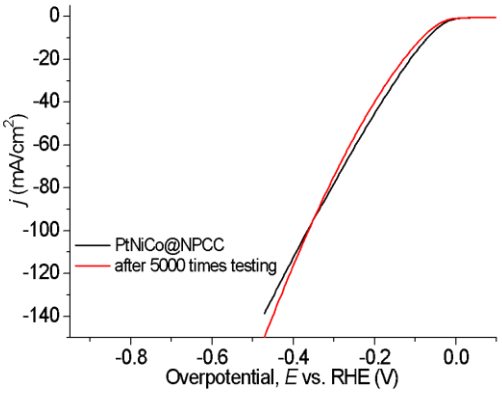

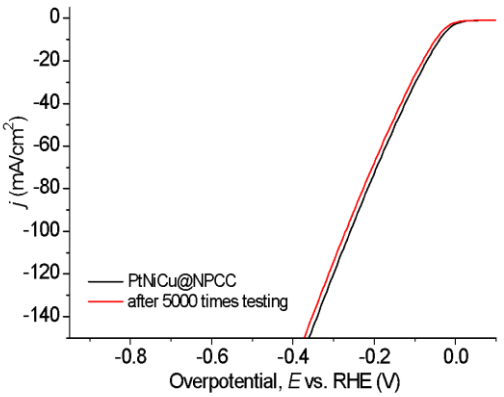

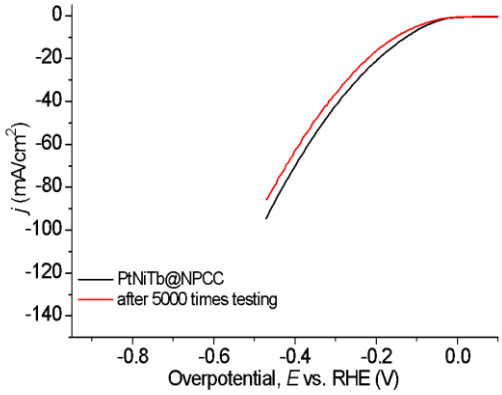

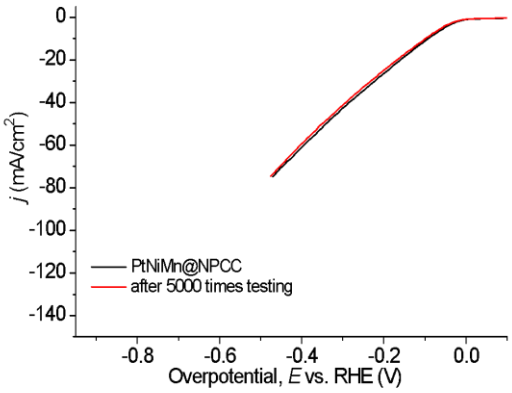

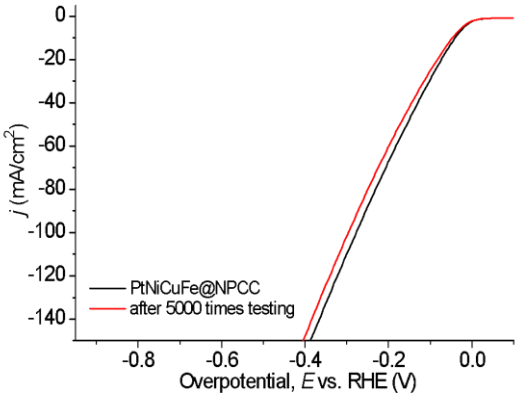

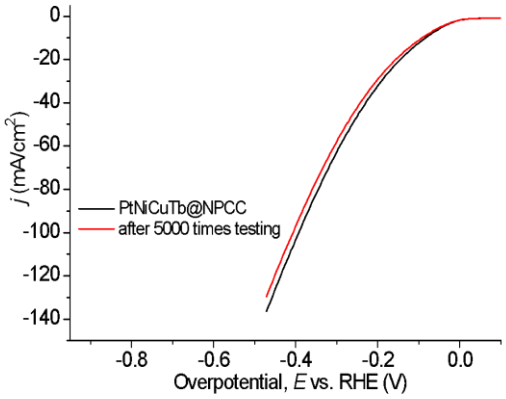

Figure S48. The polarization curves of as-synthesized samples before and after 5000 times testing for electrocatalytic hydrogen evolution with a scan rate of 5 mV/s in a 1 M KOH solution. All overpotentials are given without iR correction.

4.9 Oxygen Evolution Reaction (OER)

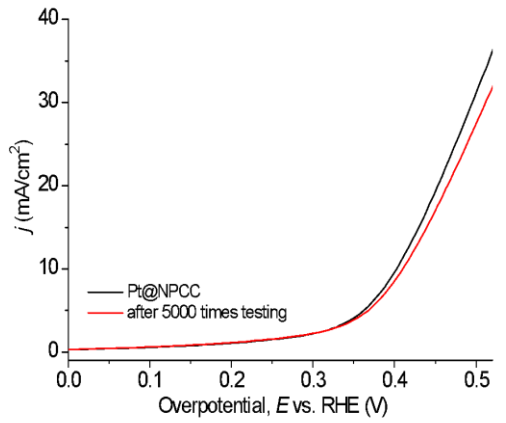

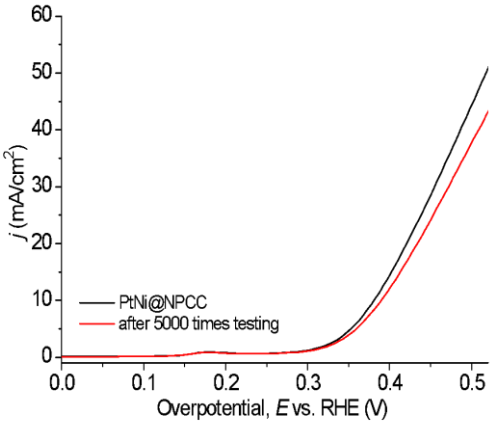

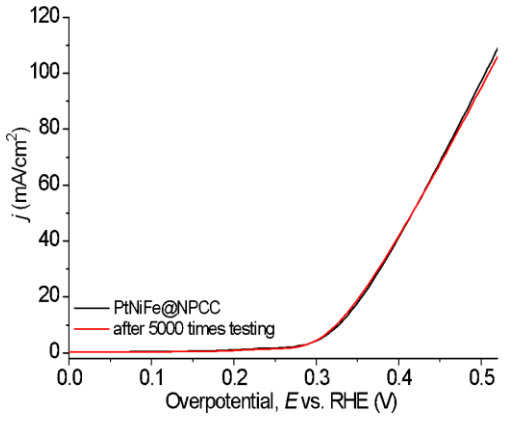

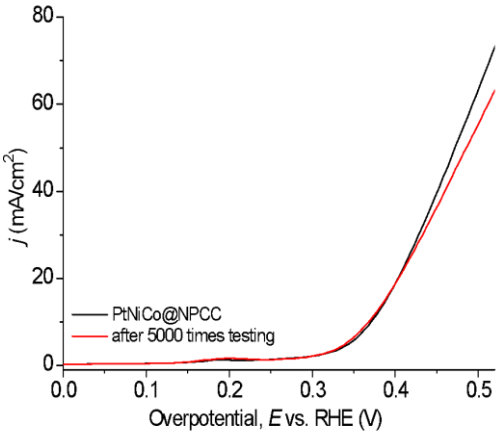

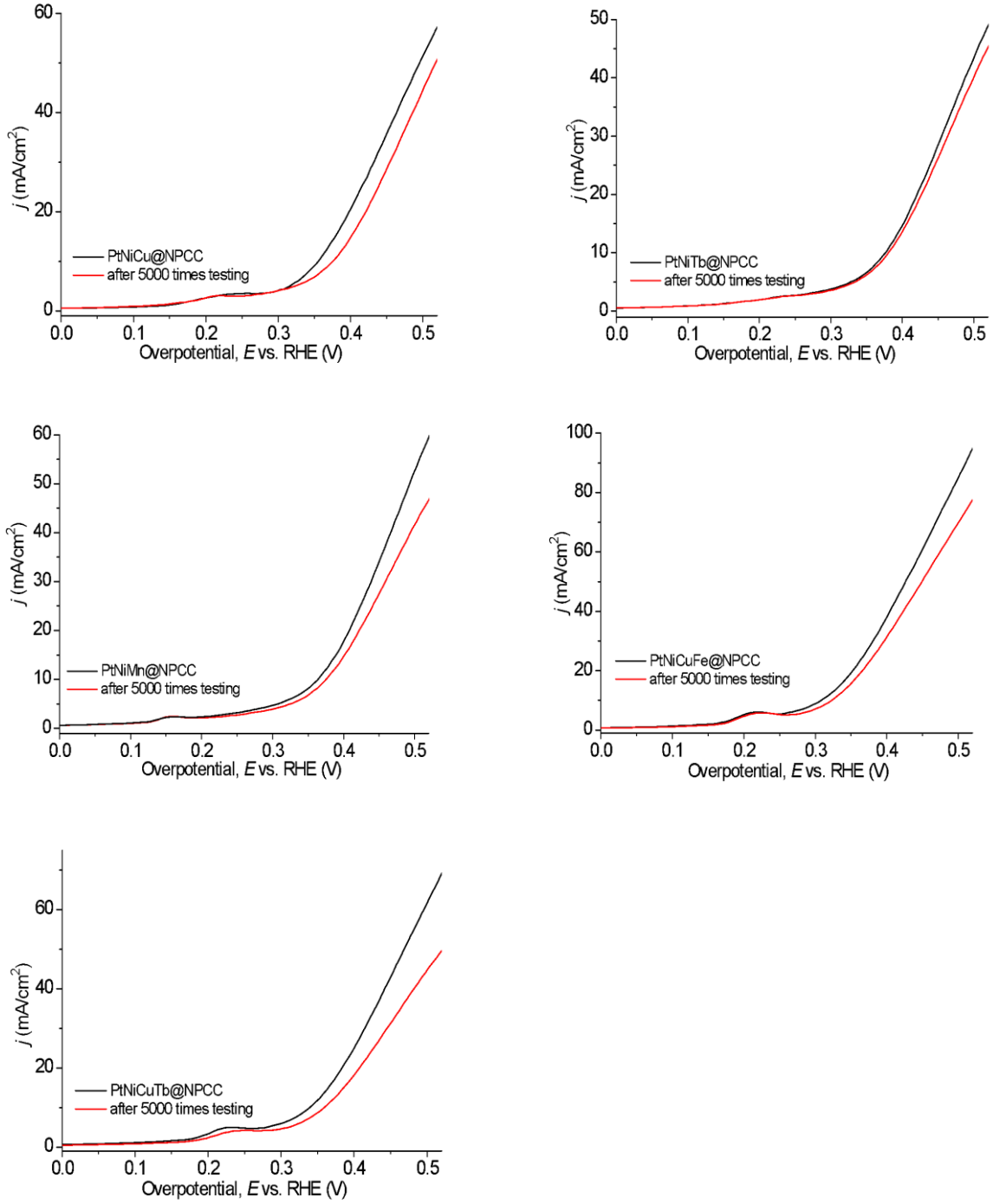

Figure S49. The polarization curves of as-synthesized samples before and after 5000 times testing for electrocatalytic oxygen evolution with a scan rate of 5 mV/s in a 1 M KOH solution. All overpotentials are used without iR correction.

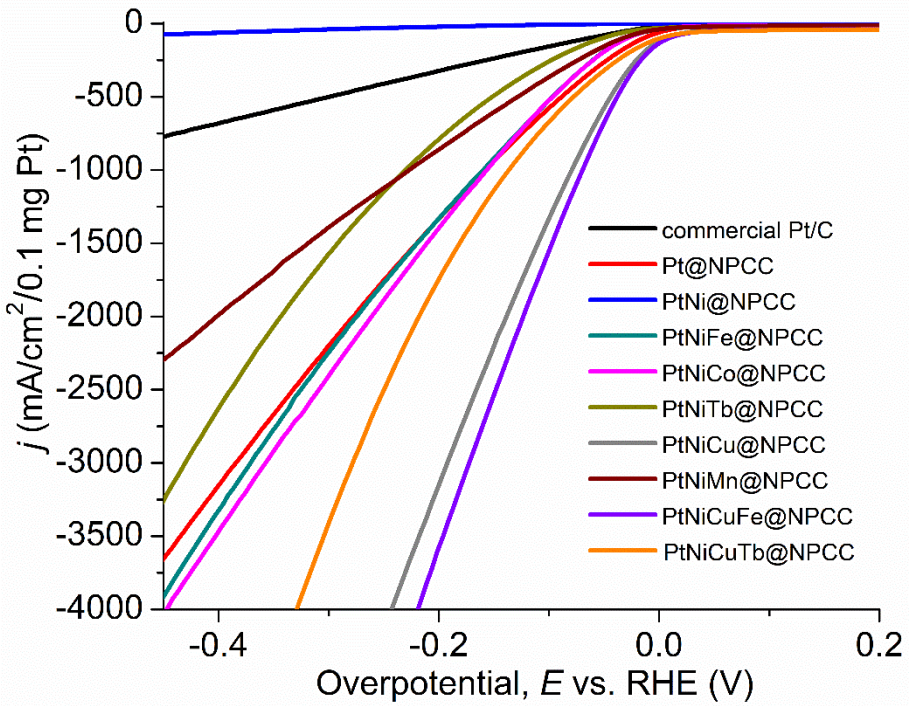

Figure S50. HER polarization curves of selected catalysts in N_2–satuated 1.0 M KOH solution (scan rate: 5 mV s^{-1}; rotation rate: 1600 rpm). All overpotentials are used without iR correction.

Table S2 Summary of the electrocatalytic HER performance of the materials reported herein and compared to selected high-performance materials from the literature.

catalyst	overpotential (mV)	electrolyte	reference
Pt@NPCC	30 (at j = 10 mA cm^{-2})	1 M KOH	This work
PtNiCu@NPCC	38 (at j = 10 mA cm^{-2})	1 M KOH	This work
PtNiFe@NPCC	83 (at j = 10 mA cm^{-2})	1 M KOH	This work
PtNiCo@NPCC	69 (at j = 10 mA cm^{-2})	1 M KOH	This work
PtNiCuFe@NPCC	40 (at j = 10 mA cm^{-2})	1 M KOH	This work
Au@PdAg NRBs	26.2 (at j = 10 mA cm^{-2})	0.5 M H_2SO_4	*J. Am. Chem. Soc.* **2016**, *138*, 1414
Pt–Ni excavated nano-multipods	65 (at j = 10 mA cm^{-2})	0.1 M KOH	*Nat. Commun.* **2017**, *8*, 15131
Pt-islands/Pt(111) surface	~140 (at j = 4 mA cm^{-2})	0.1 M KOH	*Science* **2011**, *334*, 1256
$Ni(OH)_2$/Pt-islands/Pt(111) surface	~110 (at j = 4 mA cm^{-2})	0.1 M KOH	*Science* **2011**, *334*, 1256
Pt(111)/$Co(OH)_2$	159 (at j = 4 mA cm^{-2})	0.1 M KOH	*Nat. Mater.* **2012**, *11*, 550
$Ni(OH)_2$ modified Ir	~61 (at j = 4 mA cm^{-2})	0.1 M KOH	*Angew. Chem. Int. Ed.* **2012**, *51*, 12495
$Ni(OH)_2$ modified Pt	~95 (at j = 4 mA cm^{-2})	0.1 M KOH	*Angew. Chem. Int. Ed.* **2012**, *51*, 12495
Pt electrode	~70 (at j = 4 mA cm^{-2})	0.1 M KOH	*Energy Environ. Sci.* **2013**, *6*, 1509
Pt_3Ni frames/$Ni(OH)_2$/C	~59 (at j = 4 mA cm^{-2})	0.1 M KOH	*Science* **2014**, *343*, 1339
Nickel–Silver alloy	~260 (at j = 4 mA cm^{-2})	0.1 M KOH	*Phys. Chem. Chem. Phys.* **2014**, *16*, 19250
Pt NWs/SL-$Ni(OH)_2$	85.5 (at j = 4 mA cm^{-2})	0.1 M KOH	*Nat. Commun.* **2015**, *6*, 6430

Table S3 Summary of the electrocatalytic OER performance of the materials reported herein and compared to selected high-performance materials from the literature.

catalyst	overpotential η at j = 10 mA cm^{-2} (mV)	electrolyte	reference
PtNiFe@NPCC	330	1 M KOH	This work
PtNiCo@NPCC	370	1 M KOH	This work
PtNiCu@NPCC	350	1 M KOH	This work
PtNiCuTb@NPCC	340	1 M KOH	This work
PtNiCuFe@NPCC	300	1 M KOH	This work
IrO_2	427	1 M KOH	*J. Am. Chem. Soc.* **2012**, *134*, 17253.
IrO_x	320	1 M KOH	*J. Am. Chem. Soc.* **2013**, *135*, 16977.
IrO_2	338	1 M KOH	*Nat. Commun.* **2014**, *5*, 4477
IrO_2	330	1 M KOH	*Angew. Chem. Int. Ed.* **2015**, *54*, 8722.

Ru-(a)	290	1 M KOH	*J. Am. Chem. Soc.* **2015**, *137*, 4347.
RuO_2	358	0.5 M KOH	*ACS Nano*, **2015**, *9*, 1977
Ir−Ni mixed oxide	~310	0.1 M $HClO_4$	*J. Am. Chem. Soc.* **2015**, *137*, 13031
$IrNiO_x$@Meso-ATO	~340	0.05 M H_2SO_4	*Angew. Chem. Int. Ed.* **2015**, *54*, 2975
$Ni(OH)_2$−Au (light)	270	1 M KOH	*J. Am. Chem. Soc.* **2016**, *138*, 9128

References

(1) Venna, S. R.; Jasinski, J. B.; Carreon, M. A. Structural Evolution of Zeolitic Imidazolate Framework-8. *J. Am. Chem. Soc.* **2010**, *132*, 18030-18033.
(2) Teranishi, T.; Hosoe, M.; Tanaka, T.; Miyake, M. Size Control of Monodispersed Pt Nanoparticles and Their 2D Organization by Electrophoretic Deposition. *J. Phys. Chem. B* **1999**, *103*, 3818-3827.